

Exchange flow of two immiscible fluids and the principle of maximum flux

R. R. KERSWELL

School of Mathematics, University of Bristol, University Walk, Bristol BS8 1TW

(Received 7 April 2011)

The steady, coaxial flow in which two immiscible, incompressible fluids of differing densities move past each other slowly in a vertical cylindrical tube has a continuum of possibilities due to the arbitrariness of the interface between the fluids. By invoking the presence of surface tension to at least restrict the shape of any interface to that of a circular arc or full circle, we consider the following question: which flow will maximise the exchange when there is only one dividing interface Γ ? Surprisingly, the answer differs fundamentally from the better-known co-directional two-phase flow situation where an axisymmetric (concentric) core-annular solution always optimises the flux. Instead, the maximal flux state is invariably asymmetric either being a ‘side-by-side’ configuration where Γ starts and finishes at the tube wall or an *eccentric* core-annular flow where Γ is an off-centre full circle in which the more viscous fluid is surrounded by the less viscous fluid. The side-by-side solution is the most efficient exchanger for a small viscosity ratio $\beta \lesssim 4.60$ with an eccentric core-annular solution optimal otherwise. At large β , this eccentric solution provides 51% more flux than the axisymmetric core-annular flow which is always a local minimiser of the flux.

1. Introduction

For Newtonian fluids at least where the governing Navier-Stokes equations are known, the most fundamental issue in fluid mechanics is predicting the realised flow solution for a given initial state and set of boundary conditions against a background of omnipresent noise. Non-uniqueness of solution is endemic due to the nonlinearity of the Navier-Stokes equations but even in special limits (e.g. vanishing Reynolds number or steady, unidirectional flow) where these simplify to the linear Stokes’ equations, degeneracy is rife when finding the flow domain is part of the problem. A well-known example of this is the pressure-driven flow of two immiscible fluids along a cylindrical tube (e.g. Everage 1973, Joseph, Renardy & Renardy 1984, Joseph, Nguyen and Beavers 1984, and Joseph et al. 1997). Here there is a continuum of steady unidirectional solutions possible due to the arbitrariness in the interface between the two fluids. In practice, however, the less viscous fluid usually tries to encapsulate the more viscous fluid shielding it from the stationary tube walls. The resultant core-annular solution with the more viscous fluid surrounded by the less viscous fluid has been observed for fluid combinations ranging from oil and water (Charles & Redberger 1962, Yu & Sparrow 1967, Hasson, Mann & Nir 1970), to molten polymers (Southern & Ballman 1973, Everage 1973, Lee & White 1974, Williams 1975 and Minagawa & White 1975).

Interestingly, it appears that if an extra constraint is added to the system - that the mean volumetric flux along the tube vanishes - different steady solutions can be observed (Arakeri et al. 2000, Huppert & Hallworth 2007, Beckett et al. 2011). Such a flow is easily

set up in the laboratory by placing a tank of dense fluid directly above a tank full of less dense fluid and connecting the two by a vertical cylindrical tube. If the density difference or the tube cross-section is small enough or the fluid viscosities large enough, it is reasonable to anticipate a steady, coaxial flow established in the tube in which the denser fluid falls under gravity displacing the less dense fluid upwards. When the lower tank is initially full and both fluids incompressible, this exchange flow is constrained to have no net volume flux along the tube. As in the unidirectional flow situation, the form of the steady, coaxial two-fluid flow realised is fascinatingly unclear due to the arbitrariness of the interface between the fluids (formally, any union of open curves terminating on the tube wall and closed curves in the interior are possible). Using salty and pure water, Arakeri et al (2000) saw only a ‘half-and-half’ solution where the interface divides the tube cross-section into two approximately equal domains (hereafter referred to as a ‘side-by-side’ solution). In contrast, Huppert & Hallworth (2007) report seeing only a concentric core-annular flow as their steady low-Reynolds solution and recently both types of flow have been seen in the same apparatus (Beckett et al. 2011). Beyond its intrinsic interest, this flow has applications ranging from the exchange of degassed and gas-rich magma in volcanoes (Kazahaya, Shinohara & Saito 1994, Stevenson & Blake 1998, Huppert & Hallworth 2007, Beckett et al. 2011) to plug-cementing oil wells (e.g. Frigaard & Scherzer 1998, Moyers-Gonzalez & Frigaard 2004). There is also associated work on exchange flow problems involving miscible fluids, tilted tubes or channels, and unsteady solutions (see the recent articles by Seon et al. 2007, Znaïen et al. 2009 and Taghavi et al. 2009 for references).

In the volcano degassing problem, gas-rich, less-dense magma rises in a volcano conduit, at some upper height releases its gas and then falls as denser, degassed magma creating a convective overturning flow. A central modelling issue in constraining degassing rates is estimating the individual volumetric flux of the gas-rich magma as a function of relevant parameters (e.g. Huppert & Hallworth 2007). So far a flux parametrisation based upon axisymmetric core-annular exchange flow in a cylindrical vent has been assumed (e.g. Kazahaya, Shinohara & Saito 1994, Stevenson & Blake 1998) but the observation of distinctly different side-by-side flows evidently casts doubt upon doing this. Clearly the flux rates generated by these side-by-side flows needs to be calculated in order to assess whether a significantly different flux parametrization may be more relevant. This was the initial motivation for the present study. While carrying this out, however, it was hard to resist conjecturing that of all the possible exchange flows, the realised flow is the one which maximises the individual volumetric flux, or in other words, is most ‘efficient at exchanging’. While admittedly ad-hoc, such a maximum flux selection ‘principle’ has proved useful in predicting the encapsulation phenomenon in the 2-fluid unidirectional flow problem (Maclean 1973, Everage 1973, Joseph, Renardy & Renardy 1984, Joseph, Nguyen & Beavers 1984). In the words of Joseph, Nguyen and Beavers (1984) “our experiments show that something like this is going on” (see also Charles & Redberger 1962, Yu & Sparrow 1967, Hasson, Mann & Nir 1970, Southern & Ballman 1973, Everage 1973, Lee & White 1974, Williams 1975, Minagawa & White 1975). Joseph, Renardy & Renardy (1984), however, add some qualifications: this state can become unstable if the more viscous core gets too small, emphasizing that the principle is far from infallible.

The maximum flux principle for the 2-fluid unidirectional problem is posed for fixed applied pressure gradient which can take any value. It is exact if the interface is specified (see Appendix A) but becomes heuristic if the interface is included as part of the optimisation procedure. In the exchange flow problem, the pressure gradient is set up by the flow to be greater than that needed to hydrostatically support the less dense fluid but less than that needed to support the more dense fluid. Since its precise value

is *a priori* unknown, it makes sense in exploring a predictive hypothesis to also seek the maximum individual flux over all possible pressure gradients as well as interfaces. This means that while the maximum (now individual) flux principle is again exact for given pressure gradient and interface (see Appendix A), the extension to optimising over flow field, interface *and* pressure gradient again relegates the ‘principle’ to a hypothesis. Nevertheless, this still warrants examination given the insight provided by such a conjecture in the 2-fluid unidirectional problem and the difficulty in pursuing the alternative. Technically, resolving the flow degeneracy requires knowledge of the initial conditions, the pressure boundary conditions set-up across the tube and the inherent instability mechanisms present. Pragmatically, the initial conditions are never known that well (e.g. barriers are slid open or plugs removed in the laboratory), the pressure gradient which gets set up difficult to measure and assessing the stability of the evolving flow which leads to a given steady state impossible without access to very difficult direct numerical simulations (e.g. some slip must be allowed at the walls to get exchange and experiments indicate that the initially-horizontal interface quickly becomes sharply folded on release).

Formally solving the maximum individual flux optimisation problem with the interface (or interfaces) as an unknown is a formidable challenge not attempted here. Rather, a survey is conducted over a physically-motivated subspace of all mathematically-possible steady, coaxial solutions. This subspace is defined by two (mild) assumptions: a) the fluids occupy one (possibly multi-connected) domain so that there is only one interface Γ , and b) that this interface is a circular arc or a full circle. The motivation for the former assumption is stability - multiple small fluid domains would presumably aggregate - and the presence of some surface tension between the two fluids conveniently motivates the latter. The axially-constant, lateral pressure difference required to balance interfacial tension, however, will be ignored in what follows as it has no consequence for the calculations.

2. Formulation

Consider two immiscible fluids with densities ρ_1 and ρ_2 and viscosities μ_1 and μ_2 which are flowing in a vertical circular tube of radius a across which there is a pressure gradient G ($= -dp/dz > 0$) and g is the acceleration due to gravity. Assuming that fluid 1(2) occupies an area $A_1^*(A_2^*)$, the Navier-Stokes equations for steady exchange flow of the two fluids either directed up or down the tube (so the problem is just in the cross-sectional plane) are

$$-G = \mu_1 \nabla^2 u_1^* - \rho_1 g \quad \text{in } A_1^*, \quad -G = \mu_2 \nabla^2 u_2^* - \rho_2 g \quad \text{in } A_2^* \quad (2.1)$$

with non-slip boundary conditions at the tube wall and continuity of velocity and stress at the interface Γ^* between the two fluids, that is

$$u_1^* = u_2^* \quad \& \quad \mu_1 \frac{\partial u_1^*}{\partial n} = \mu_2 \frac{\partial u_2^*}{\partial n} \quad \text{on } \Gamma^* \quad (2.2)$$

(where $\partial/\partial n$ is the normal derivative to Γ^*). There is a further constraint that the net volume flux through the tube is zero so

$$Q^* := - \int u_1^* dA_1^* = \int u_2^* dA_2^*. \quad (2.3)$$

Without loss of generality, we assume $\rho_1 > \rho_2$ so that Q^* is positive (the less dense fluid rises). This does not prejudice the choice of viscosities later because of the symmetry

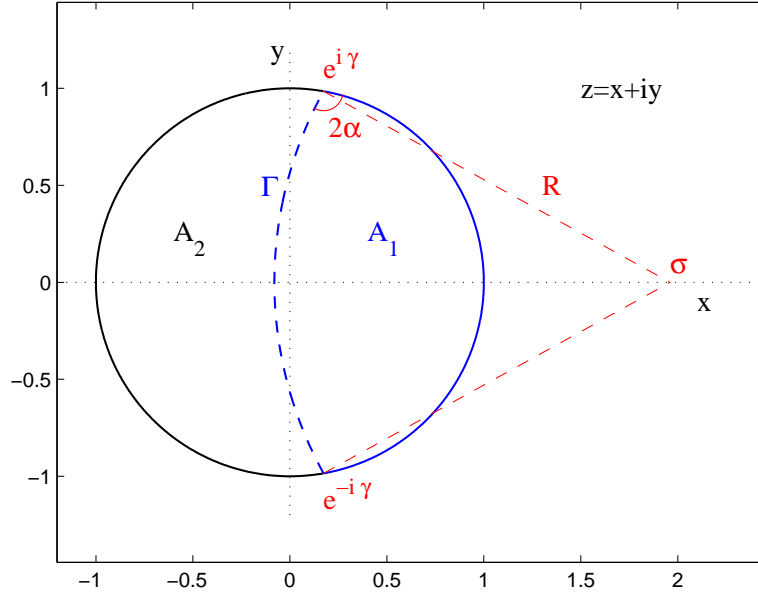


FIGURE 1. The side-by-side solution configuration specified by two parameters: γ and α .

$(\rho_1, \rho_2, g) \rightarrow (\rho_2, \rho_1, -g)$: the direction ‘up’ is irrelevant with only the density difference being important.

The system is non-dimensionalised (*’s removed) using the tube radius a , the differential hydrostatic pressure gradient $\Delta\rho g$ (where $\Delta\rho := \rho_1 - \rho_2$) and μ_1 so that after defining λ by

$$G = \frac{1}{2}(\rho_1 + \rho_2)g - \frac{1}{2}\Delta\rho g\lambda \quad (2.4)$$

then

$$\nabla^2 u_1 = \lambda + 1 \quad \text{in } A_1, \quad (2.5)$$

$$\beta \nabla^2 u_2 = \lambda - 1 \quad \text{in } A_2, \quad (2.6)$$

$$u_1 = u_2 \quad \& \quad \frac{\partial u_1}{\partial n} = \beta \frac{\partial u_2}{\partial n} \quad \text{on } \Gamma. \quad (2.7)$$

where

$$\beta := \frac{\mu_2}{\mu_1}. \quad (2.8)$$

Henceforth u_1 and u_2 are in units of $\frac{1}{2}\Delta\rho g a^2/\mu_1$ and the one-fluid volume flux

$$Q := - \int u_1 dA_1 = \int u_2 dA_2 \quad (2.9)$$

is in units of $\frac{1}{2}\Delta\rho g a^4/\mu_1$ with $A_1 \cup A_2$ being the unit disk. It is worth remarking that the system (2.5)-(2.7) for a *given* Γ is really the linear combination of two problems (e.g. take the limiting values $\lambda = -1$ and 1). Neither will respect the flux balance condition (2.9) but a unique (convex) linear combination with $\lambda \in (-1, 1)$ will.

Two specific choices are now made for Γ motivated by the likely presence of some surface tension which would make the interface have constant curvature. The first is a

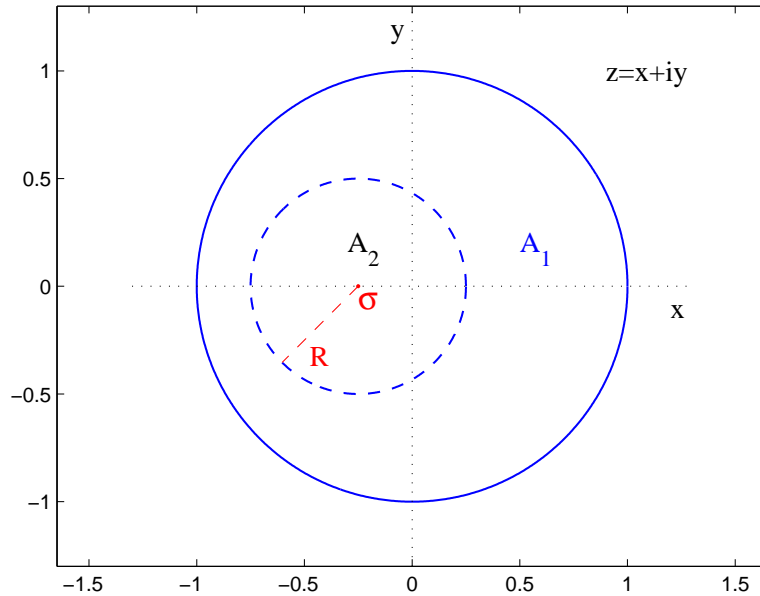


FIGURE 2. The eccentric core-annular configuration specified by two parameters: σ and R .

circular arc of general curvature and position which intersects the tube wall so that the two fluids are next to each other - the *side-by-side* solution: see figure 1. The second is a full circle completely contained within, but not concentric with, the tube so that one fluid encapsulates the other - the *eccentric* core-annular solution: see figure 2. The limiting case of a *concentric* core-annular solution needs to be treated separately but is easily solved analytically.

There has been a long history of work in the multiphase literature on 2-fluid *unidirectional* flow (typically referred to as ‘stratified pipe flow’ - Ng, Lawrence & Hewitt 2002 give a nice review) and many of the techniques of solution are equally applicable to the current exchange flow problem. For example, Russell & Charles (1959) appear the first to have considered the concentric flow possible in a circular pipe. Then, with horizontal pipelines in mind, the interface was often assumed planar (Semenov & Tochigin 1962, Gemmill & Epstein 1962, Yu & Sparrow 1967, Packham & Shail 1971, Ranger & Davis 1979, Hall 1992, Hall & Hewitt 1993, Biberg & Halvorsen 2000). More general interfaces of constant curvature as treated here were first considered theoretically by Bentwich and coworkers (Bentwich 1964, 1976, Bentwich, Kelly & Epstein 1970) using a bipolar coordinate transformation and more recently by Brauner, Rovinsky & Maron (1996) and Rovinsky, Brauner & Maron (1997). The calculations performed here were formulated in ignorance of this body of work and inevitably employ different techniques. The upside, of course, of developing two different formulations (one based upon Poisson’s integral formula for the circular arc interface flows - see Appendix B - and the other on a conformal transformation for the full circle interface flows - see Appendix C) is that they were able to cross-validate each other. Interestingly, in the 2-fluid unidirectional problem, the interface shape has also been derived by minimising the free energy (Bentwich 1976, Gorelik & Brauner 1999 and Ng, Lawrence & Hewitt 2002) with the conclusion that the

circular arc assumption is a good approximation in all practical situations (e.g. Gorelik & Brauner 1999). This suggests that our survey over circular arc interfaces should yield a good assessment of the possible fluxes.

2.1. Side-by-side solutions

The geometry of the side-by-side solution is shown in figure 1 to be defined by two parameters: γ , the (upper) intercept latitude of Γ with the tube wall, and 2α , the angle between Γ and tube wall. For given viscosity ratio β and pressure gradient λ , one of these (nominally α) is determined by the flux balance leaving a 1-dimensional family of side-by-side flows with corresponding fluxes $Q = Q_s(\beta, \lambda; \gamma)$ possible (see appendix B for the calculation details). There is a symmetry

$$Q(\beta, \lambda; \gamma, \alpha) = \frac{1}{\beta} Q\left(\frac{1}{\beta}, -\lambda; \pi - \gamma, \frac{\pi}{2} - \alpha\right) \quad (2.10)$$

which means that only $\beta \geq 1$ need be considered providing the full ranges of γ and α are studied. Henceforth fluid 2 will always be the more viscous fluid so that the non-dimensionalisation has been done using the smaller dynamic viscosity μ_1 .

2.2. Eccentric solutions

The eccentric core-annular solution has one fluid domain as a totally-contained circular disk (cylinder) not touching the tube wall. The radius $R < 1$ and centre $(\sigma, 0)$ of Γ define the geometry uniquely up to obvious rotations and reflections. To match smoothly onto the choices made in the side-by-side solution, σ is chosen to be +ve(-ve) for A_1 in A_2 (A_2 in A_1). As before, for given viscosity ratio β and pressure gradient λ , one of these two geometrical parameters is determined by the flux balance. This is done by searching over R for given

$$d := \begin{cases} 1 + \sigma - R & A_2 \text{ in } A_1 & \sigma < 0 \\ -1 + \sigma + R & A_1 \text{ in } A_2 & \sigma > 0 \end{cases} \quad (2.11)$$

which either represents the positive displacement from $(-1, 0)$ to $(\sigma - R, 0)$, the leftmost point of Γ for the case of A_2 in A_1 ($\sigma < 0$), or the negative displacement of $(\sigma + R, 0)$, the rightmost point of Γ , from $(1, 0)$ for the case of A_1 in A_2 ($\sigma > 0$). This choice is made for two reasons. Firstly, d is a convenient way of extending the side-by-side solutions continuously beyond their pinch-off points into the corresponding eccentric solutions: $\gamma \rightarrow 0$ corresponds to A_2 encapsulating A_1 and d decreasing across zero whereas $\gamma \rightarrow \pi$ corresponds to A_1 encapsulating A_2 and d increasing across zero (see figure 3). Secondly, only one flux-balanced solution was ever found for a given d whereas some σ can have two flux-balanced solutions. The result is that two 1-dimensional families of eccentric core-annular flows with corresponding fluxes $Q_e(\beta, \lambda; d)$ (more viscous core) and $\hat{Q}_e(\beta, \lambda, d)$ (less viscous core) are possible (see appendix C for the calculation details). It's worth re-emphasizing here that $\beta \geq 1$ so all the flux values quoted are in units of $1/\mu_1$ where μ_1 is the smaller dynamic viscosity.

2.3. Concentric solutions

When Γ is a circle concentric with the tube wall there is a simple solution to the problem (2.5)-(2.7) discussed recently by Huppert & Hallworth (2007):

$$u_1 = \frac{\lambda + 1}{4}(r^2 - 1) - R^2 \log r, \quad R \leq r \leq 1 \quad (2.12)$$

$$u_2 = \frac{\lambda - 1}{4\beta}(r^2 - R^2) - R^2 \log R - \frac{\lambda + 1}{4}(1 - R^2). \quad r \leq R \quad (2.13)$$

The associated fluxes are

$$Q_1 = \frac{\pi}{8} \left[(\lambda + 1)(2R^2 - R^4 - 1) + 4R^2(1 - R^2) + 8R^4 \log R \right], \quad (2.14)$$

$$Q_2 = \frac{\pi}{8\beta} \left[(1 - \lambda)R^4 - 2\beta(1 + \lambda)R^2(1 - R^2) - 8\beta R^4 \log R \right]. \quad (2.15)$$

Since this is a special case of an eccentric core-annular solution with $\sigma = 0$, there is a unique $0 < R < 1$ for a flux-balanced solution which is

$$R_c = \sqrt{\frac{2\beta - \sqrt{4\beta^2 - \beta(1 + \lambda)[\beta(3 - \lambda) + (\lambda - 1)]}}{[\beta(3 - \lambda) + (\lambda - 1)]}} \quad (2.16)$$

so that the flux (for fluid 2 in the core) is $Q_c(\beta, \lambda)$. As $\beta \rightarrow \infty$ and maximising over λ ,

$$R_c \rightarrow \sqrt{(1 + \lambda)/(3 - \lambda)}, \quad \lambda \rightarrow 0.1746 \quad Q_c \rightarrow 0.01831 \quad (2.17)$$

from above. The flux for the opposite scenario of the less viscous fluid (fluid 1) in the core, \hat{Q}_c , is retrieved by setting $\beta \rightarrow 1/\beta$ in expressions (2.14) and (2.15) and multiplying Q by $1/\beta$ to convert the flux units to those using the smaller dynamic viscosity. As $\beta \rightarrow \infty$ and maximising over λ ,

$$R_c \sim \sqrt[4]{\frac{2}{\beta(1 - \lambda)}}, \quad \lambda = 1 - O(\beta^{-1/3}) \quad \text{and} \quad \hat{Q}_c \rightarrow \frac{1}{4}\pi/\beta \approx 0.7854/\beta \quad (2.18)$$

from below. (It is worth remarking at this point that Huppert & Hallworth (2007) order their flows by the starting upper-and-lower-viscosity ratio γ_h (the subscript h is to distinguish this γ with our use here as an angle). Together with their assumption that the lower fluid always rises in the centre, this means that their Te (Huppert & Hallworth 2007, eqn (3.5)) is related to Q here as follows

$$Te = \begin{cases} \frac{1}{2}\beta\hat{Q}_c & \text{less viscous fluid in core} & \gamma_h \gg 1 & \rightarrow \pi/8 \\ \frac{1}{2}Q_c & \text{more viscous fluid in core} & \gamma_h \ll 1 & \rightarrow 0.00915. \end{cases}$$

2.4. Strategy

The strategy now is to calculate $\max_{\lambda} Q$ as a function of β over all possible geometries smoothly ranging from the concentric solution with *less* viscous fluid in the core through to the concentric solution with the *more* viscous fluid in the core. Figure 3 illustrates the spectrum of possibilities and a glimpse of how the flux varies at one β value. Before detailing the results further, the reader may be amused by an admission. At onset, this author (naively?) expected the calculation of maximum flux to be a simple competition between a local maximum achieved by the side-by-side solution and the flux Q_c associated with the concentric core-annular flow influenced by the known behaviour of unidirectional 2-fluid flow. The side-by-side solution, however, quickly loses its interior maximum ($0 < \gamma < \pi$) as β increases in favour of an end-point maximum at $\gamma = \pi$. The fact that this end-point maximum *exceeds* the concentric solution flux Q_c unequivocally indicated the importance of the intermediate eccentric core-annular flux Q_e . (This is also seen in a simple 1D analogue problem outlined in appendix D.)

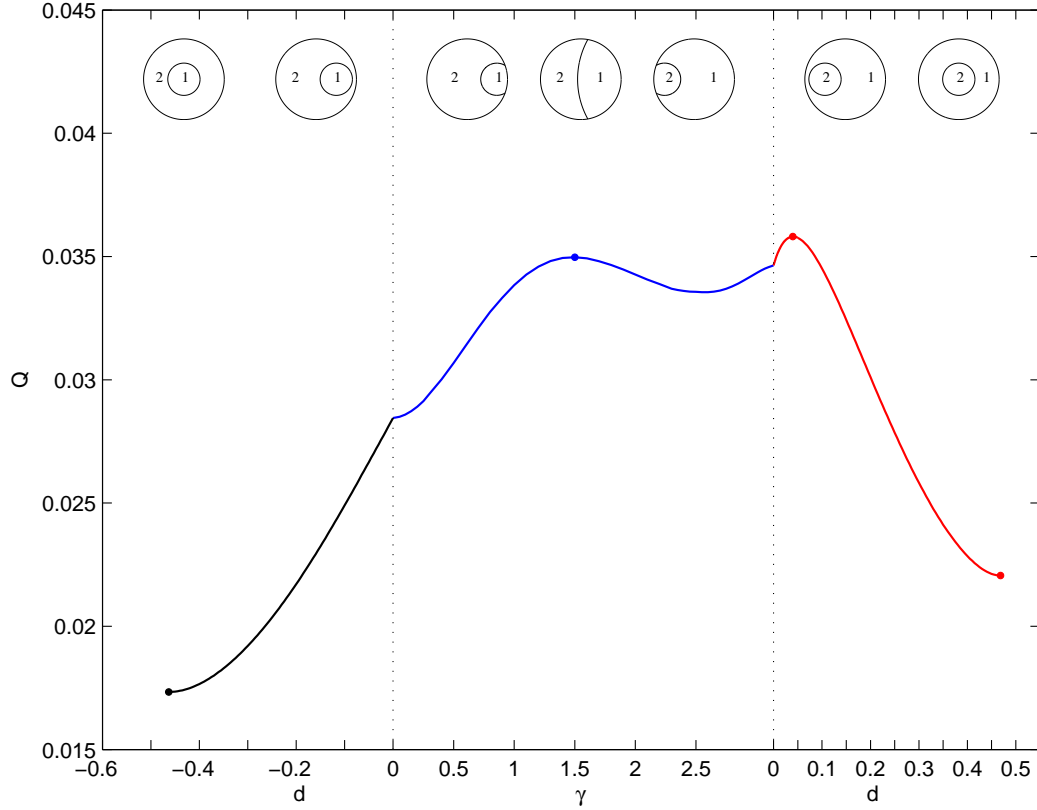


FIGURE 3. The flux $\max_{\lambda} Q$ plotted across the various flow configurations ($d < 0$ indicates less viscous core and $d > 0$ more viscous core) for $\beta = 5$. The leftmost point is \hat{Q}_c , beyond this, the region $d < 0$ is the domain for \hat{Q}_e , the region $\gamma \in [0, \pi]$ is the domain for Q_s , $d > 0$ the domain for Q_e and the rightmost point is \hat{Q}_c . The interior local maxima are highlighted with dots. The curve is only C^0 because the abscissa changes character at $\gamma = 0$ and π of course.

3. Results

There is a special case of the problem which can be solved using known results. When $\beta = 1$, the optimal balanced flow of fluid 1 must mirror that in fluid 2. In particular, $\lambda = 0$, Γ is the diameter $x = 0$ and $u = 0$ on Γ . The problems for either fluid then decouple into single phase pressure-driven flow in a ‘half’-cylinder (semicircular cross-section). The flux is 0.07438920 in our non-dimensional units according to White’s (1991) equation (3-44). This provides an excellent test of the side-by-side computations (see Table 1 which shows 3 significant figure correspondence although there is really 5). Further checks are available between the very different side-by-side and eccentric flow codes by examining the limit in which the encapsulated fluid approaches the duct wall and one of the side-

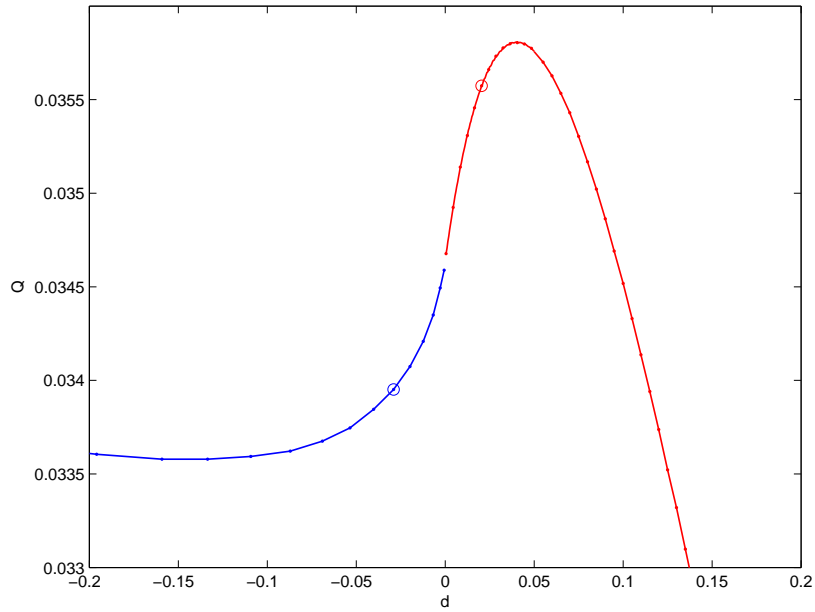


FIGURE 4. Plotting $\max_{\lambda} Q$ against d at $\beta = 5$ for side-by-side solutions as $d \rightarrow 0^-$ ($\gamma \rightarrow \pi$) and eccentric solutions as $d \rightarrow 0^+$ demonstrates the smooth connection between the two formulations. Velocity fields for the circled points are shown in figure 5.

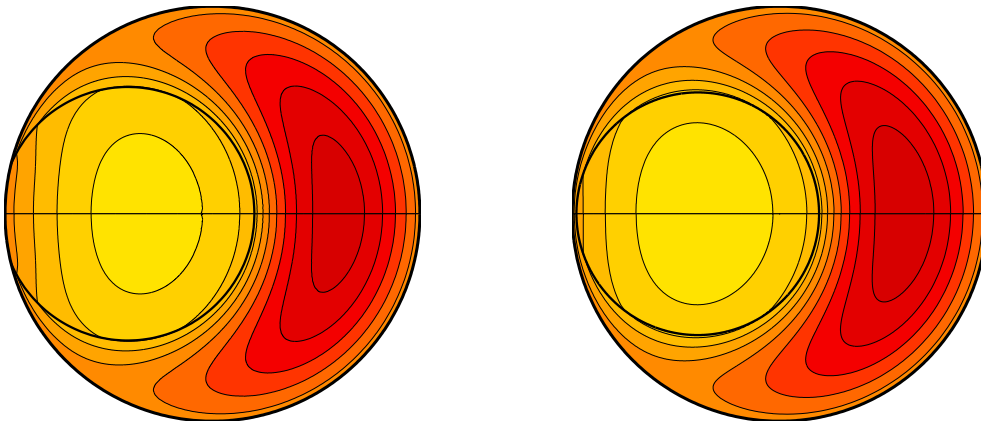


FIGURE 5. The pinching-off side-by-side ($d = -0.0198$, $-0.051 \leq u \leq 0.041$) and near-touching eccentric solutions ($d = 0.0205$, $-0.052 \leq u \leq 0.043$) for $\beta = 5$ and the optimal $\lambda = -0.20$ corresponding to the circles in figure 4. The contours range from -0.105 (dark/red) to 0.105 (light/white) in steps of 0.01 here and throughout figures 7 and 8 to aid comparison.

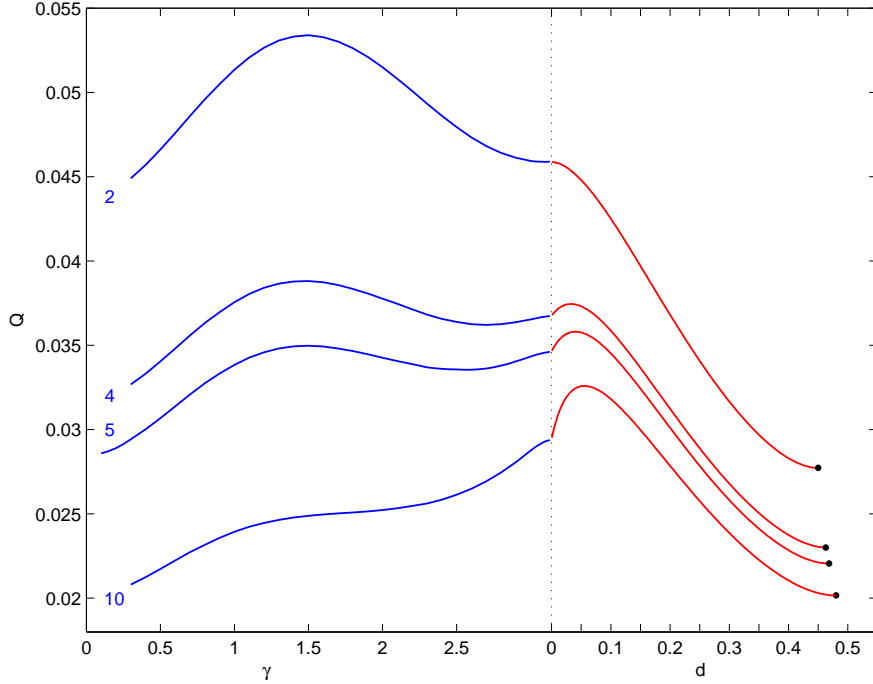


FIGURE 6. $\max_{\lambda} Q$ as a function of γ for the side-by-side solutions and as a function of $d > 0$ for the eccentric solutions at $\beta = 2, 4, 5$ and 10 . The single dot at the right end of each curve corresponds to the concentric case Q_c . The global flux maximum is a side-by-side solution for $\beta \leq 4.60$ and an eccentric solution for $\beta \geq 4.60$.

by-side domains pinches off (e.g. figure 4 where using d as the abscissa shows at least C^1 continuity in $\max_{\lambda} Q$ at $\gamma = \pi$ or $d = 0$ at $\beta = 5$). The two codes have to be pushed hard to demonstrate consistency across this singular configuration which can be treated properly using a unipolar transformation (see the work of Rovinsky, Brauner & Maron 1997 in the unidirectional problem).

3.1. $\max_{\lambda} Q$

The β value chosen in figure 3 has been purposely chosen to show the presence of flux maxima in the side-by-side solutions and the ($d > 0$ or more viscous fluid in the core) eccentric solutions (Q_e). The complementary eccentric solutions with the less viscous fluid in the core (\hat{Q}_e) always show monotonic behaviour in which the flux decreases from the $\gamma = 0$ side-by-side value down to the concentric core-annular value of \hat{Q}_c (leftmost point or most negative d). This uninteresting part of the flux spectrum is suppressed in figure 6 to focus on $\max_{\lambda} Q$ over γ and $d > 0$ for $\beta \in [2, 10]$ over which all the interesting behaviour occurs. At $\beta = 1$, the side-by-side solution with $\gamma = \pi/2$ and $\alpha = \pi/4$ supplies the only flux maximum with both concentric core-annular solutions being global minima as $Q_c = \hat{Q}_c$. At $\beta \approx 2$, a local maximum starts to appear in the eccentric solutions with d small and positive (see figure 6). At $\beta \approx 4.60$, this ‘eccentric’ maximum becomes the global maximum with the ‘side-by-side’ local maximum disappearing by $\beta \approx 8.2$. Thereafter the sole flux maximum is always an eccentric solution. Figures 7 and 8 show how the maxima change with β including an eccentric optimal flux solution at $\beta = 10,000$.

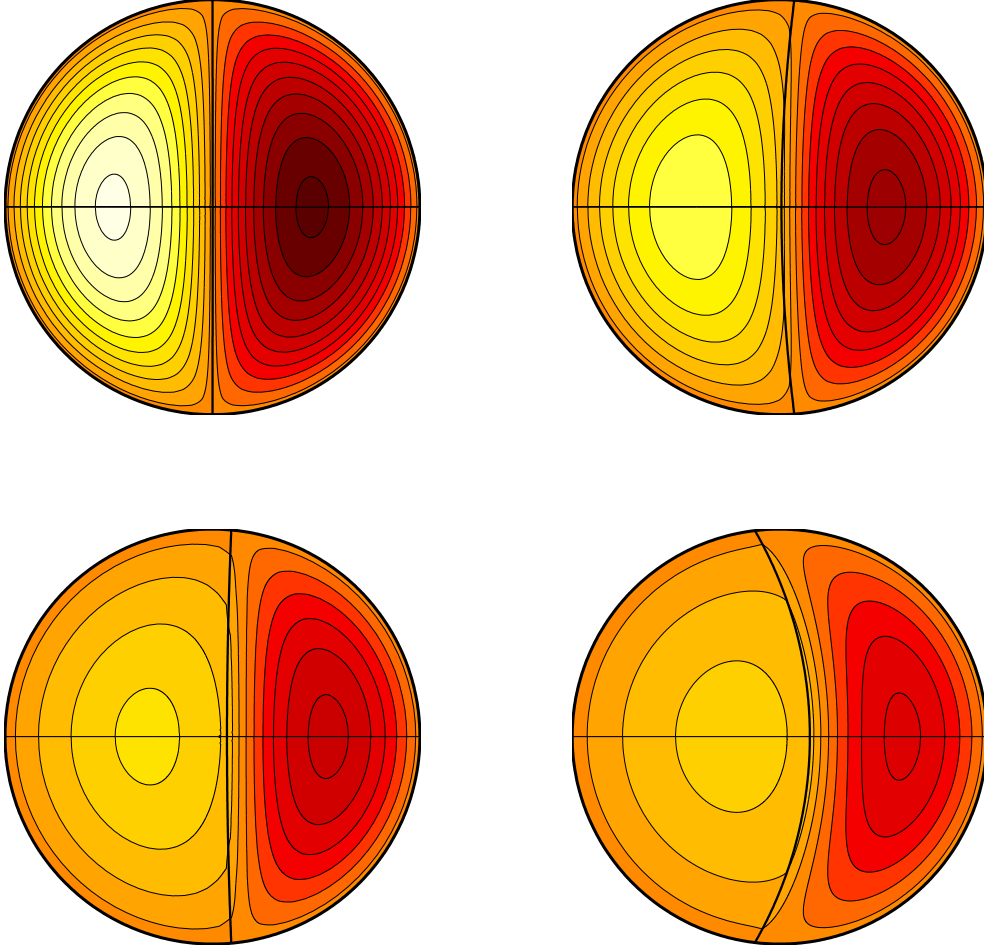


FIGURE 7. Maximal flux side-by-side solutions for $\beta = 1$ (top left, $-0.098 \leq u \leq -0.098$), $\beta = 2$ (top right, $-0.078 \leq u \leq 0.063$), $\beta = 5$ (bottom left, $-0.058 \leq u \leq 0.037$) and $\beta = 8$ (bottom right, $-0.047 \leq u \leq 0.029$). The contours range from -0.105(dark/red) to 0.105 (light/white) in steps of 0.01 here and throughout figures 5 and 8 to aid comparison.

This confirms that the optimal asymptotic solution has plug flow for the more viscous core. Figure 9 plots the maxima values as a function of β highlighting the cross-over point at $\beta \approx 4.60$ (see also Tables 1 and 2). The concentric core-annular flux values for the more viscous fluid in the core Q_c and less viscous fluid in the core \hat{Q}_c are also shown as a local and global minima respectively.

3.2. $\max_{\lambda} Q$ for $\beta \rightarrow \infty$

At large β , there is every reason to suspect that the maximal flux possible possesses a simple expansion around its limiting value:

$$\max_{\lambda, d} Q_e(\beta, \lambda; d) = Q_{\infty} + \frac{a_1}{\beta} + \frac{a_2}{\beta^2} + \dots \quad (3.1)$$

β	λ	γ	α	$Q_s (\times 10^{-2})$
1	0.00	1.57	0.785	7.44
1.5	-0.06	1.52	0.810	6.11
2	-0.10	1.50	0.812	5.34
2.5	-0.13	1.48	0.814	4.82
3	-0.15	1.46	0.813	4.43
3.5	-0.18	1.46	0.809	4.13
4	-0.19	1.47	0.786	3.88
4.5	-0.21	1.47	0.779	3.67
5	-0.22	1.48	0.761	3.50
6	-0.25	1.52	0.721	3.21
7	-0.27	1.58	0.668	2.98
8	-0.28	1.69	0.585	2.79

TABLE 1. $\max_{\lambda,\gamma} Q_s$ (Q for the side-by-side solution) as a function of β . The maximum is unique global for $\beta < 4.60$ and thereafter is a local maximum until it vanishes for a $\beta \approx 8.2$.

β	λ	σ	R	$Q_e (\times 10^{-2})$
2.5	-0.140	-0.393	0.594	4.25
3	-0.155	-0.390	0.590	4.02
3.5	-0.168	-0.387	0.584	3.86
4	-0.180	-0.387	0.582	3.74
4.5	-0.188	-0.386	0.578	3.65
5	-0.198	-0.386	0.574	3.58
6	-0.209	-0.385	0.570	3.47
7	-0.211	-0.382	0.568	3.40
8	-0.222	-0.383	0.565	3.34
9	-0.225	-0.383	0.564	3.29
10	-0.226	-0.381	0.563	3.26
15	-0.246	-0.383	0.555	3.15
20	-0.245	-0.381	0.556	3.10
50	-0.260	-0.381	0.549	3.01
100	-0.260	-0.380	0.551	2.98
200	-0.263	-0.381	0.550	2.96
500	-0.263	-0.3795	0.5485	2.9544
1000	-0.263	-0.3794	0.5476	2.9514
2000	-0.263	-0.3797	0.5473	2.9499
5000	-0.263	-0.3795	0.5479	2.9490
10000	-0.263	-0.3795	0.5479	2.9487
∞	-0.263	-0.3795	0.5480	2.9484

TABLE 2. $\max_{\lambda,d} Q_e$ (Q for the eccentric solution) as a function of β . The maximum appears for $\beta \approx 2$, is a local maximum for $2 \lesssim \beta < 4.60$ and becomes a unique global maximum for $\beta > 4.60$.

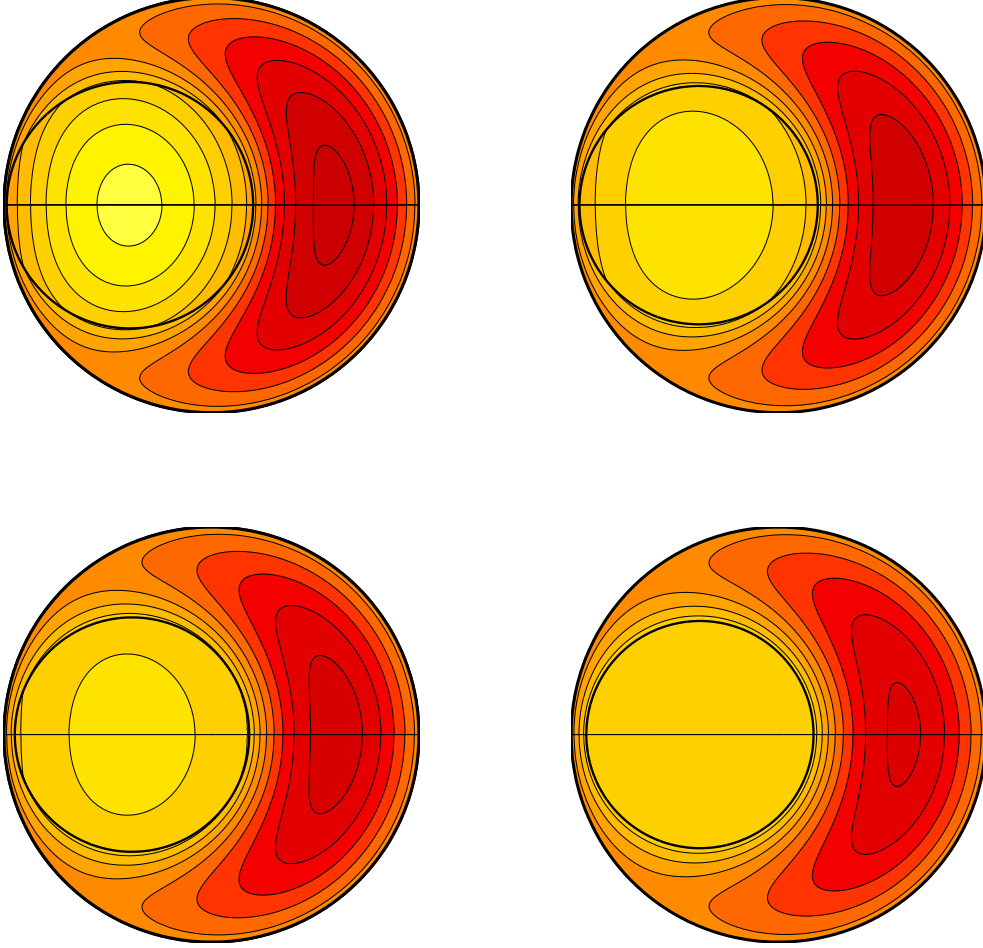


FIGURE 8. Maximal flux eccentric core-annular solutions for $\beta = 2.5$ (top left, $-0.059 \leq u \leq 0.058$), $\beta = 5$ (top right, $-0.053 \leq u \leq 0.044$), $\beta = 8$ (bottom left, $-0.051 \leq u \leq 0.039$) and $\beta = 10,000$ (bottom right, $-0.047 \leq u \leq 0.031$). The contours range from -0.105 (dark/red) to 0.105 (light/white) in steps of 0.01 here and throughout figures 5 and 7 to aid comparison.

The scalars Q_∞ and a_1 can be estimated as follows

$$Q_\infty \approx \frac{\beta_1 Q(\beta_1) - \beta_2 Q(\beta_2)}{\beta_1 - \beta_2} \quad a_1 \approx \frac{\beta_1 \beta_2}{\beta_2 - \beta_1} \left[Q(\beta_1) - Q(\beta_2) \right] \quad (3.2)$$

where β_1 and β_2 have suitably large values. There is good evidence that $Q_\infty \approx 2.9484 \times 10^{-2}$ and $a_1 \approx 3.00 \times 10^{-2}$ supporting the original assumption: see figure 10. Another check on this value of Q_∞ is available by artificially imposing plug flow in the core (e.g. see the lower right solution in figure 8: note also this limit has applications in the unidirectional situation, e.g. Hodgson & Charles 1963, Kruyer, Redberger & Ellis 1967). The matching conditions at Γ then simplify to just continuity $u_1 = u_2$ and the condition that the continuation of u_1 into A_2 has no logarithmic singularities ($\oint_\Gamma \mathbf{dx} \cdot \nabla u_1 = 0$)

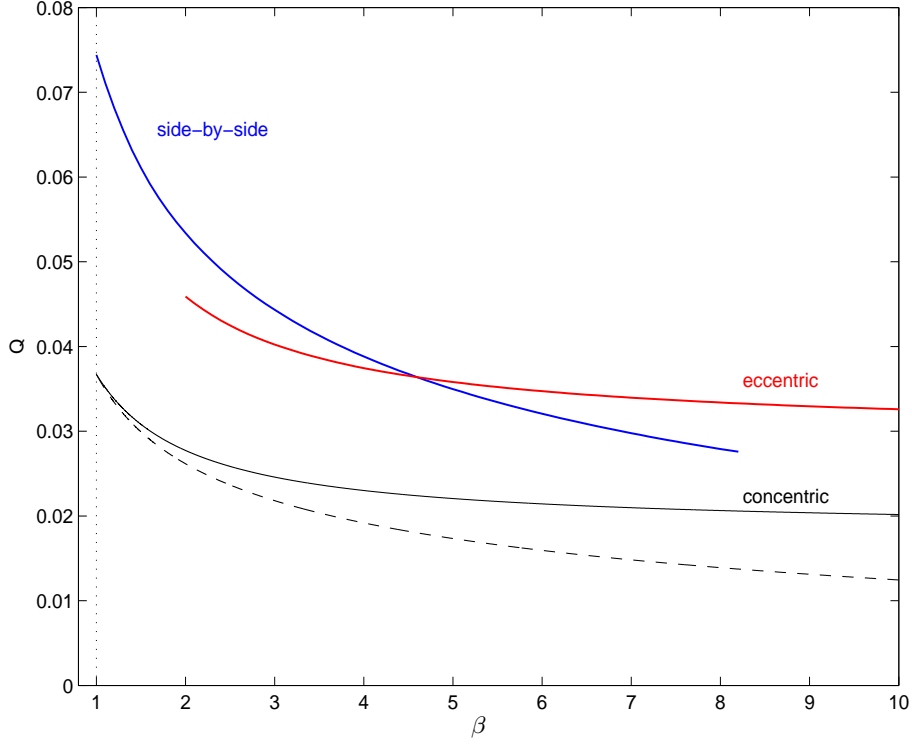


FIGURE 9. $\max_{\lambda, \gamma} Q_s$ (left upper blue curve), $\max_{\lambda, d} Q_e$ (right upper red curve) and $\max_{\lambda} Q_c$ (lowest solid black curve) compared as a function of β . The side-by-side maximum disappears for $\beta \gtrsim 8.2$ and the eccentric solution only starts to have a maximum for $\beta \gtrsim 2$. The lowest dashed (black) curve corresponds to $\max_{\lambda} \hat{Q}_c$, the global minimum of the more viscous fluid encapsulating the less viscous solution.

which eliminates β from the problem. A straightforward search over λ and σ then reveals the maximum of $Q_{\infty} = 2.94844 \times 10^{-2}$ at $\lambda = -0.263$, $\sigma = -0.3795$, $R = 0.54798$ (and $d = 1 + \sigma - R = 0.0725$).

3.3. $Q(\beta, \lambda)$ for fixed λ

So far all the results shown have been optimised over the pressure gradient λ . The presumption is that, in the absence of any explicitly imposed gradient, the flow sets up its own to maximum the volumetric exchange. Figure 11 shows the effect of fixing λ on the flux profile at $\beta = 5$. The same general trends emerge with one important additional feature highlighted by the $\lambda = -0.5$ curve. Here \hat{Q}_c (leftmost point) is approximately the same as Q_c (rightmost point). Figure 12 plots the two core-annular flux functions Q_c and \hat{Q}_c against λ to show that the less-viscous core solution flux \hat{Q}_c actually exceeds the more-viscous core solution flux Q_c for $\lambda \lesssim -0.51$ at $\beta = 5$. This threshold pressure gradient monotonically decreases as β increases to, for example, ≈ -0.89 at $\beta = 100$ (recall $-1 < \lambda < 1$): see figure 12. Since a λ value of -1 translates into a pressure gradient which hydrostatically maintains the denser fluid, the conclusion is that the less-viscous-fluid-in-the-core concentric solution is favoured over its complement for large enough pressure gradients.

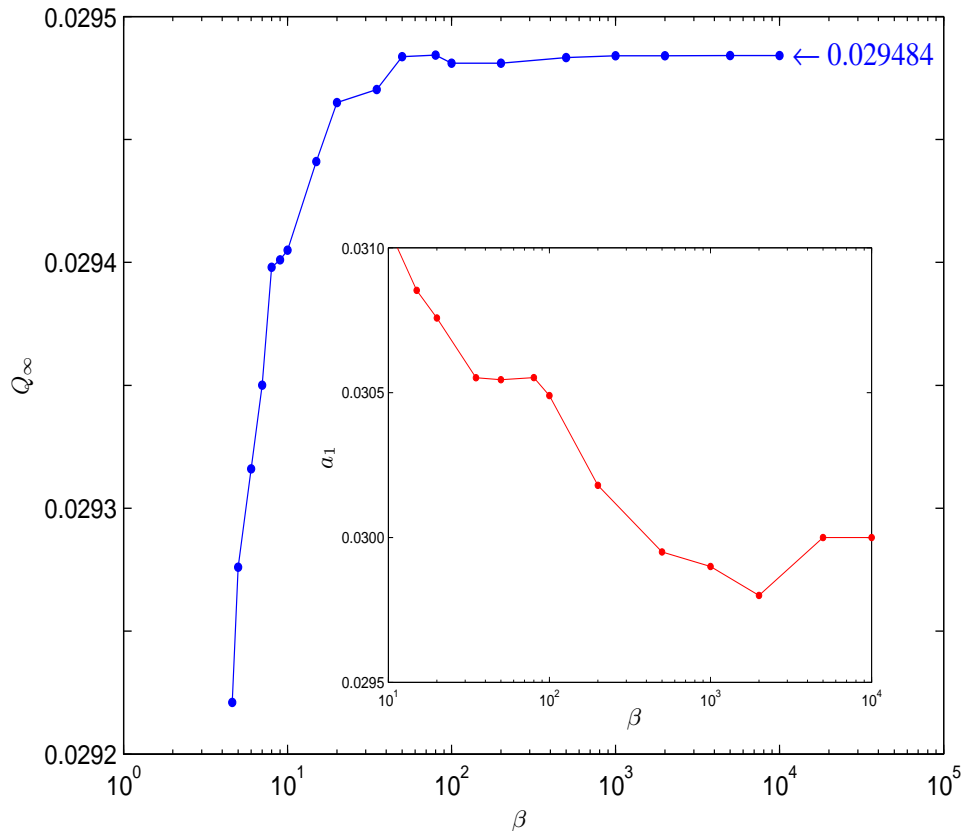


FIGURE 10. The coefficients Q_∞ and a_1 (inset) as calculated using the expressions (3.2) against β where β and the next smallest value of β were used.

4. Discussion

This paper has considered the steady, coaxial flow of two immiscible fluids of different densities and viscosities in a straight vertical cylindrical tube such that their volumetric fluxes balance. Assuming that the interface between the two fluids is either a circular arc or a full circle, the main conclusion is that the flow which optimises the volumetric flux over all possible pressure gradients is always asymmetric (the same is true in a simple 1D model too: see appendix D). This seems a surprising result given that the variational problem itself allows axisymmetric solutions and is presumably a result of the restricted form of the interface allowed. Mathematically, the fact that Γ is not permitted to generate ‘homogenized’ regions in which the two fluids are alternately layered to form a composite may preclude the existence of an optimal which shares the same symmetry as the variational problem itself. Precisely this type of optimal emerges for 2-fluid unidirectional flow in a square duct (or in the equivalent optimal design problem of placing two elastic

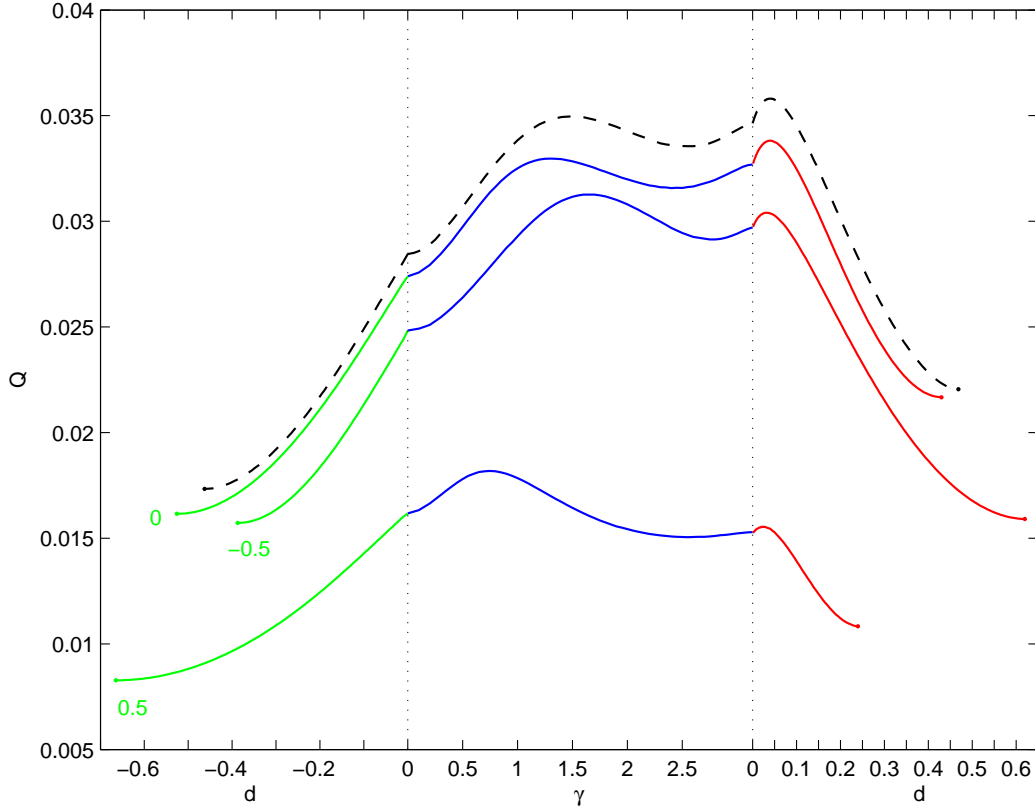


FIGURE 11. The effect of fixing the pressure gradient λ at -0.5 , 0 and 0.5 on Q for $\beta = 5$. The (black) dashed upper envelope is the result of optimising over λ as shown in figure 6.

materials in a square rod for maximum torsional rigidity): e.g Goodman, Kohn & Reyna (1986) (note, in contrast, that the flux maximiser for the 2-fluid unidirectional problem in a circular disk can be proven to be a simple axisymmetric core-annular flow - Joseph, Renardy & Renardy 1984).

Physically, based upon what one would expect to see, the restriction imposed on the interface, however, seems entirely reasonable. Then, for viscosity ratios $\lesssim 4.60$ the optimal flow is a side-by-side solution in which each fluid makes contact with a side of the tube and otherwise is an *eccentric* core-annular solution with the more viscous fluid encapsulated by the less viscous fluid. (In fact, in this latter case, the eccentricity is so marked, that it could look like a side-by-side solution from one direction to the unwary.) The axisymmetric (concentric) core-annular solution in which one fluid encircles the other is surprisingly either a local or global minimiser of the flux. The clear conclusion is that displacing the core of such a flow to one side increases the flux by allowing the outer fluid to ‘bulge’

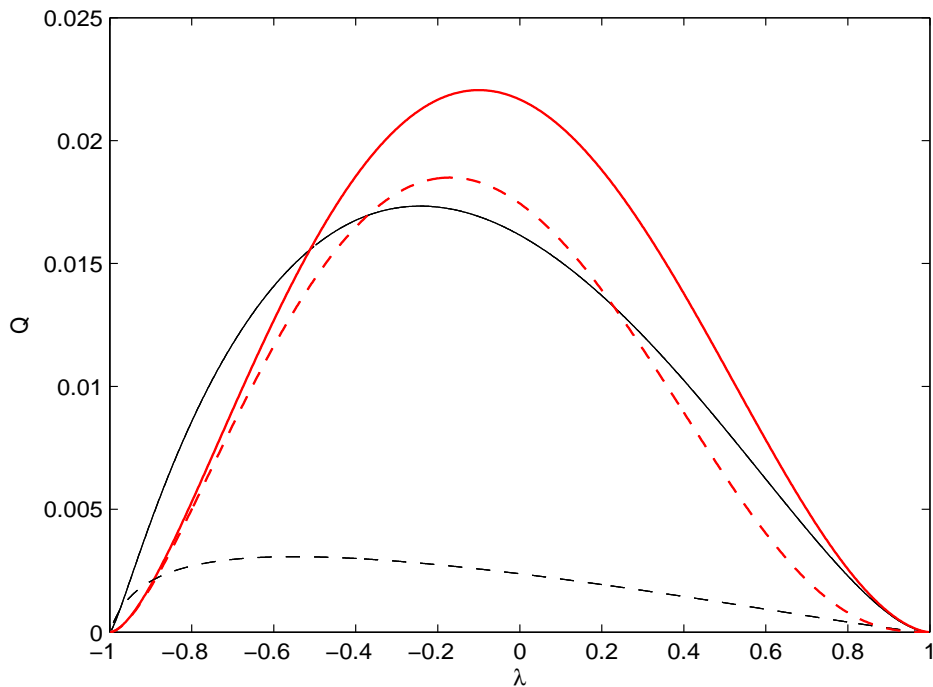


FIGURE 12. The concentric core-annular fluxes $Q_c(\beta, \lambda)$ and $\hat{Q}_c(\beta, \lambda)$ plotted against λ for $\beta = 5$ (thick solid red and thin solid black respectively) and $\beta = 100$ (thick dashed red and thin dashed black respectively). The crossing of the solid lines at ≈ -0.51 is consistent with figure 11 where $Q_c \approx \hat{Q}_c$ at $\lambda = -0.5$. The dashed lines cross at $\lambda \approx -0.89$ for a ratio of 100.

through the larger gap. This generalises the equivalent observation made for the flow of a single fluid through an eccentric annulus duct (see figure 3-8 on page 127 of White 1991).

The fact that the principle of maximum flux predicts a side-by-side solution at low viscosity ratios does find general support in the work of Arakeri et al (2000) and Beckett et al. (2011) (see their figure 4). However, Huppert & Hallworth (2007) never mention seeing a side-by-side solution during their low-viscosity-ratio experiments, instead reporting only a steady concentric core-annular flow. More intriguing, however, is that in their observations of the core-annular solution, Huppert & Hallworth (2007) report that “the upward-moving less dense fluid forms an almost straight-sided column rising up the centre of the tube” presumably regardless of the viscosity ratio. For (their) $\gamma_h > 1$ this means that the less viscous fluid is in the core. This is consistent with the findings of Beckett

et al (2011) who report that “the less viscous fluid occupies the core” because all their experiments have the less dense fluid being less viscous too. From the flux perspective, the results presented here show that this configuration globally *minimises* the maximum flux over all possible geometries, i.e. core annular flow with the less viscous in the centre is the geometrical optimiser in

$$\min_{\text{geometry}} \max_{\lambda} Q.$$

This apparent contradiction is ameliorated somewhat if the pressure gradient set up is towards the maximum possible for exchange (e.g. see figure 12), but nevertheless the core-annular solution still remains a local flux minimiser. The principle of *minimum* flux then appears more useful at large viscosity ratios (e.g. see figure 10 of Beckett et al. 2011). Huppert & Hallworth (2007) had already observed this for their regime $\gamma_h > 1$ which encompasses the Beckett et al. (2011) experiments. For $\gamma_h < 1$ (more dense and less viscous upper fluid), however, they note that the more-viscous-fluid-in-the-centre core-annular solution does not fit with the data (their figure 13). Interestingly, the less-viscous-in-the-centre core-annular flux extended into this regime via $Te(\gamma_h < 1) := \gamma_h Te(\gamma_h > 1) = O(\gamma_h)$ would mimic the scaling highlighted by their best fit line of $0.01\gamma_h$.

The proper route to resolving this selection problem, of course, is careful consideration of the initial value problem and the stability of the evolving solution to the small disturbances always present. A first step in this direction would be to study the Rayleigh-Taylor instability problem in a cylindrical tube where a fluid of density ρ_1 and viscosity μ_1 fills the half cylinder $z > 0$ and a fluid of density $\rho_2 < \rho_1$ and viscosity μ_2 occupies $z < 0$. Establishing which interfacial deformation mode (axisymmetric or asymmetric) has the largest growth rate as a function of all the parameters present would presumably go some way in predicting which type of flow is initiated. However, even this calculation doesn’t seem to have been done yet although Batchelor & Nitsche (1993) come close.

In conclusion, it should be clear that there are some interesting issues surrounding the exchange flow of two fluids in a vertical tube. Even the steady immiscible problem displays an intriguing degeneracy of solution. Focussing on an *ad hoc* principle of maximum (or minimum) flux unfortunately looks to be too simplistic despite its appealing rationale and apparent success in an associated context. This means that there is no avoiding a more formal stability-based approach to explain what is seen in experiments.

5. Acknowledgements

This study was stimulated by experimental work carried out by the Volcanology group in Earth Sciences at Bristol University (Beckett et al. 2011) with whom I have had many interesting discussions. I would also like to thank Carl Dettmann for a reassuring discussion on singular integrals, Diki Porter for sharing his expertise on solving Laplace’s equation in complex geometries, one anonymous referee for very helpful comments which included alerting the author to some relevant multiphase literature, and another for suggesting the 1D analogue problem included in appendix D. (This work first appeared as <http://arxiv.org/abs/0912.0862>).

Appendix A. Maximum Flux Principles

The (dimensional) governing equation for steady unidirectional flow of one fluid in a duct of cross section A is

$$-G = \mu \nabla^2 u^* \tag{A 1}$$

where $G = -dp/dz > 0$ and u^* is the speed in the z direction which vanishes on the duct wall ∂A (compare with the 2-fluid bidirectional situation in 2.1). This system has many variational restatements based upon a fixed applied pressure gradient G but the simplest are: 1) minimize the dissipation rate for fixed flux and 2) maximise the flux for fixed dissipation rate. The first leads to the problem of finding stationary points of the functional

$$\mathcal{L}_1(u^*, \Lambda) := \int \mu |\nabla u^*|^2 + \Lambda_1 u^* dA \quad (\text{A } 2)$$

The Lagrangian multiplier Λ_1 must be set to $-2G$ to ensure the Euler-Lagrange equation for u^* reproduces (A 1), allowing the functional to be simplified to

$$L_1(u^*) := \int \mu |\nabla u^*|^2 - 2Gu^* dA. \quad (\text{A } 3)$$

It is clear for this functional that any stationary point will be a minimum as the only quadratic term in the integrand is positive definite (the value of the minimum is minus the dissipation rate). The second formulation (maximising the flux for fixed dissipation) is the problem of finding the stationary points of the functional

$$\mathcal{L}_2(u^*, \Lambda_2) := \int u^* + \Lambda_2 \mu |\nabla u^*|^2 dA. \quad (\text{A } 4)$$

This time the choice $\Lambda_2 = -1/(2G)$ needs to be made so that a maximum of

$$L_2(u^*) := \int u^* - \frac{\mu}{2G} |\nabla u^*|^2 dA. \quad (\text{A } 5)$$

is sought (since $-2GL_2 = L_1$, the two variational problems are equivalent). These variational problems can be readily extended to the uni-directional 2-fluid situation *provided* that the interface Γ^* is initially given. That is, the variational problem of maximizing the total flux functional

$$L_3(u^*) := \int u^* - \frac{\mu_1}{2G} |\nabla u^*|^2 dA_1 + \int u^* - \frac{\mu_2}{2G} |\nabla u^*|^2 dA_2 \quad (\text{A } 6)$$

over all u^* which vanish on the duct wall, are at least C^2 in A_1 and A_2 , and satisfy the matching conditions (2.2) is equivalent to solving the pdes

$$-G = \mu_1 \nabla^2 u^* \quad \text{in } A_1^*, \quad -G = \mu_2 \nabla^2 u^* \quad \text{in } A_2^* \quad (\text{A } 7)$$

with the same conditions on u^* (Everage 1973, Joseph, Renardy & Renardy 1984). Maclean (1973) and Everage (1973) then took the further step of extending the variational problem (A 6) to include the interface Γ^* as an unknown, speculating that the new (higher) maximizer would represent the physically-realised flow and interface for a given pressure gradient - the (heuristic) ‘maximum flux principle’. Joseph, Renardy & Renardy (1984) managed to solve this larger variational problem (with the added constraint of a prescribed division of cross-sectional area) for the special case of a circular disk to reveal the core-annular solution with the less-viscous fluid encapsulating the more-viscous fluid.

The variational formulation for the bidirectional exchange situation assuming fixed pressure gradient is very similar to the unidirectional case with the prescribed division of cross-sectional area constraint replaced by the no-net-flux condition. Working with the non-dimensionalised problem (2.5)-(2.9), and adopting the maximum flux version of the

selection hypothesis, then

$$\mathcal{L}_4(u, \Lambda_3, \Lambda_4, \Gamma) := \int (\Lambda_3 - 1)u + \Lambda_4 |\nabla u|^2 dA_1 + \int (\Lambda_3 + 1)u + \Lambda_4 \beta |\nabla u|^2 dA_2 \quad (\text{A } 8)$$

where Lagrange multipliers Λ_3 and Λ_4 enforce no net flux and fixed total dissipation rate respectively (note $\mathcal{L}_4(u, 0, 0, \Gamma) = 2Q$ where Q is the individual volumetric flux). Here *both* the Lagrange multipliers need to be set ($\Lambda_3 = -\lambda$ and $\Lambda_4 = -\frac{1}{2}$) to ensure that the Euler-Lagrange equation for u is correct (i.e. equations (2.5) and (2.6) in the two domains), leaving the functional

$$L_4(u, \Gamma) := \int -(\lambda + 1)u - \frac{1}{2} |\nabla u|^2 dA_1 + \int (1 - \lambda)u - \frac{1}{2} \beta |\nabla u|^2 dA_2. \quad (\text{A } 9)$$

Since Λ_3 has been set, there is now no formal requirement that the no-net-flux constraint holds. In other words, maximising L_4 over u and Γ will in general lead to an optimiser with a net flux *unless* the set of competing interfaces is suitably restricted. In both this and the unidirectional formulation, the unfounded extra step which converts an exact variational restatement of the problem into a heuristic hypothesis is extending the maximisation of the flux (or minimisation of the dissipation rate) over the interface as well as the flow field. The speculative nature of the hypothesis is, of course, only increased in the exchange flow problem if a further flux optimisation is performed over all possible pressure gradients as well.

Appendix B. Side-by-side solutions

The geometry of the side-by-side solution is shown in figure 1 to be defined by two parameters: γ , the (upper) intercept latitude of Γ with the duct wall, and 2α , the angle between Γ and duct wall. The coupled Poisson problems (2.5)-(2.7) become two Laplace problems by separating off simple inhomogeneous parts as follows

$$u_1^* = \Phi_1 + \frac{\lambda + 1}{4}(x^2 + y^2 - 1), \quad u_2^* = \Phi_2 + \frac{\lambda - 1}{4\beta}(x^2 + y^2 - 1) \quad (\text{B } 1)$$

which have been designed to leave the boundary conditions on the duct wall undisturbed. The functions Φ_1 and Φ_2 then satisfy

$$\nabla^2 \Phi_1 = 0 \quad \text{in } A_1, \quad (\text{B } 2)$$

$$\nabla^2 \Phi_2 = 0 \quad \text{in } A_2, \quad (\text{B } 3)$$

with boundary conditions

$$\Phi_1 = 0 \quad \text{on } x + iy = e^{i\psi} \quad -\gamma \leq \psi \leq \gamma \quad (\text{B } 4)$$

$$\Phi_2 = 0 \quad \text{on } x + iy = e^{i\psi} \quad \gamma \leq \psi \leq 2\pi - \gamma \quad (\text{B } 5)$$

$$\left. \begin{aligned} \Phi_1 - \Phi_2 &= \left(\frac{\lambda+1}{4} - \frac{\lambda-1}{4\beta} \right) (1 - x^2 - y^2) \\ 2 \frac{\partial}{\partial n} (\Phi_1 - \beta \Phi_2) &= \frac{\partial}{\partial n} (1 - x^2 - y^2) \end{aligned} \right\} \quad \text{on } x + iy \in \Gamma \quad (\text{B } 6)$$

Here the interface curve $\Gamma := \{z \mid z = x + iy = \sigma + Re^{i\theta}; |\theta| \leq |\theta_{max} := \gamma - 2\alpha|\}$ where

$$\sigma := -\frac{\sin 2\alpha}{\sin \theta_{max}} \quad \& \quad R := \frac{\sin \gamma}{\sin \theta_{max}} \quad (\text{B } 7)$$

are formulae for the centre $(x, y) = (\sigma, 0)$ and radius of curvature respectively valid for any pair $0 \leq 2\alpha, \gamma \leq \pi$. (The singular case $\gamma = 2\alpha$ where $R \rightarrow \infty$ so that Γ is a straight line cannot be formally handled but is never a practical problem.)

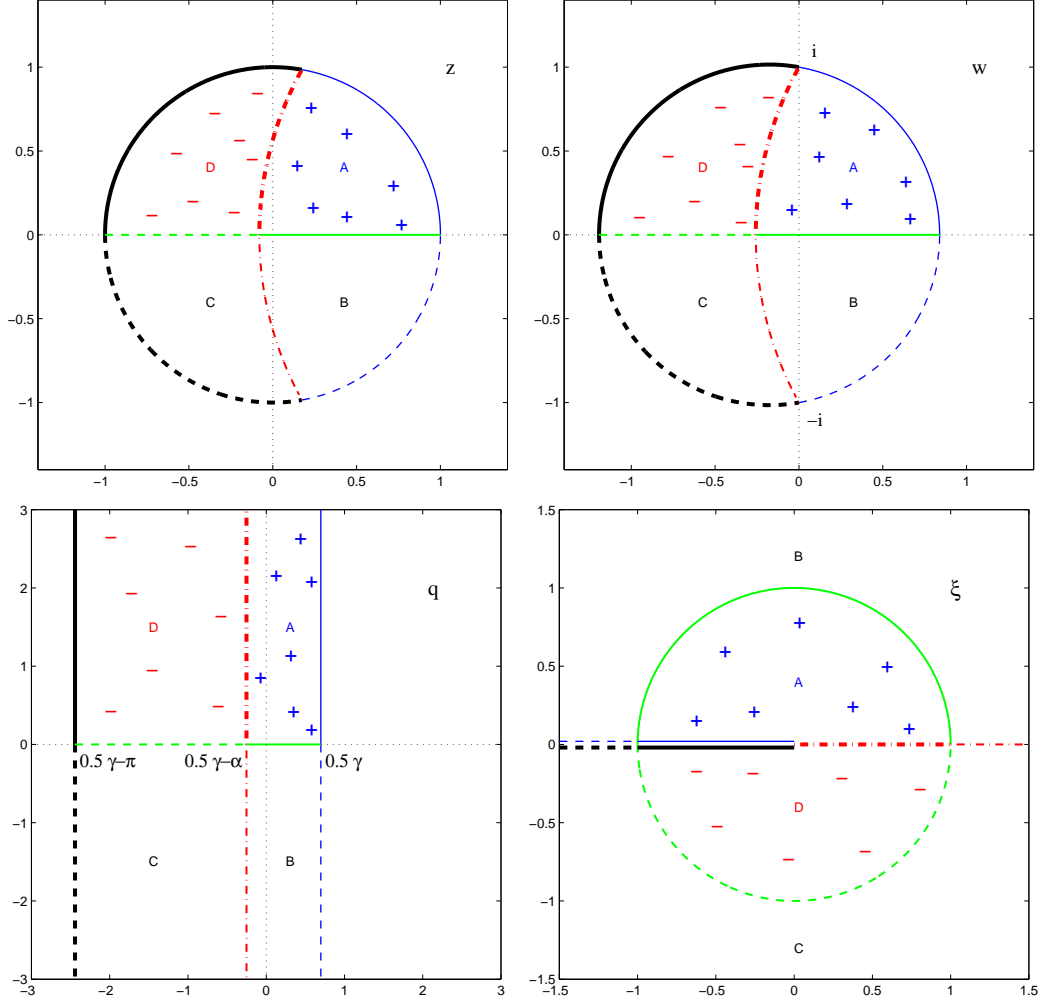


FIGURE 13. The composite conformal mapping from z to ξ . The interface curve Γ meets the duct wall at $e^{\pm i\gamma}$ in the z -plane, which are moved to $\pm i$ in the w -plane, and then to $\pm i\infty$ in the q -plane. Two separate transformations then map the strip $\frac{1}{2}\gamma - \alpha \leq \text{Re}(q) \leq \frac{1}{2}\gamma$ onto the upper half plane and the strip $\frac{1}{2}\gamma - \pi \leq \text{Re}(q) \leq \frac{1}{2}\gamma - \alpha$ onto the lower half plane. In both cases, $\text{Im}(q) > 0$ in mapped inside the appropriate unit semicircle in the ξ -plane.

The solution strategy adopted here is to transform regions A_1 and A_2 into the upper and lower half planes respectively via conformal transformations where an explicit solution can then be deduced by Poisson's integral formula. Three simple transformations prove sufficient, the first is

$$w := \frac{z - \cos \gamma}{\sin \gamma} \quad (\text{B8})$$

which rescales the duct so that its radius becomes $1/\sin \gamma$ and the 2 contact points of Γ with the duct wall $e^{\pm i\gamma}$ move to $\pm i$ (other noteworthy images are: $0 \rightarrow -\cot \gamma$, $1 \rightarrow \sin \gamma / (1 + \cos \gamma)$, $-1 \rightarrow -\sin \gamma / (1 - \cos \gamma)$; see Figure 1). A second transformation

$$q = r + is := \tan^{-1} w \quad r, s \in \Re \quad (\text{B9})$$

converts all the circular arcs into straight lines parallel to the imaginary axis in the

complex q plane. To see this, consider the transformation in reverse

$$w = \tan q = -i \frac{e^{2iq} - 1}{e^{2iq} + 1} \quad (\text{B 10})$$

and decompose this transformation into its 3 components. A strip $\frac{1}{2}\gamma - \alpha \leq r \leq \frac{1}{2}\gamma$ with $0 < \alpha \leq \pi$ is rotated through $\pi/2$ by $q \rightarrow iq$. Doubling and exponentiating $q \rightarrow iq \rightarrow e^{2iq}$ then transforms the strip into the interior of a wedge centred at the origin with sides of argument $\gamma - 2\alpha$ and γ . Finally the Möbius transformation $q \rightarrow iq \rightarrow e^{2iq} \rightarrow -i(e^{2iq} - 1)/(e^{2iq} + 1)$ converts the wedge sides into circular arcs joining the points $w = \pm i$ and the wedge interior into a circular lune with angle 2α (see Figure 1 and pages 205-207 of Marushevich 1965). The conformal transformation (B 9) is undoubtedly not the only one which would do the job (e.g. Vlasov 1986) but is particularly nice since it can be used to treat both ‘lunes’ together: A_1 maps to the strip $\frac{1}{2}\gamma - \alpha \leq r \leq \frac{1}{2}\gamma$ and A_2 maps into the strip $\frac{1}{2}\gamma - \frac{1}{2}\pi \leq r \leq \frac{1}{2}\gamma - \alpha$ in the q -plane. The intersection $A_1 \cap A_2 = \Gamma$ is then the line $\Re(q) = r = \frac{1}{2}\gamma - \alpha$.

The final transformation does, however, need tailoring to each domain separately as follows

$$\xi = \xi_1(q) := e^{i\pi(2q - \gamma + 2\alpha)/2\alpha} \quad q \in A_1 \quad (\text{B 11})$$

$$\xi = \xi_2(q) := e^{i\pi(2q - \gamma + 2\alpha)/(\pi - 2\alpha)} \quad q \in A_2 \quad (\text{B 12})$$

so that the final composition transformations are

$$\xi_1(z) := \exp\left(\frac{i\pi}{\alpha}[\tan^{-1} w(z) - \frac{1}{2}\gamma + \alpha]\right), \quad (\text{B 13})$$

$$\xi_2(z) := \exp\left(\frac{i\pi}{\frac{1}{2}\pi - \alpha}[\tan^{-1} w(z) - \frac{1}{2}\gamma + \alpha]\right) \quad (\text{B 14})$$

where

$$w(z) = \frac{z - \cos \gamma}{\sin \gamma} = \frac{e^{i\theta} - \cos(2\alpha - \gamma)}{\sin(\gamma - 2\alpha)}. \quad (\text{B 15})$$

The image of A_1/A_2 is designed as the upper/lower half ξ -plane and Γ remains a shared boundary (see Figure 1). If we define $\xi = \zeta + i\eta$ and $\bar{\Phi}_i(\zeta(x, y), \eta(x, y)) := \Phi_i(x, y)$ ($i = 1, 2$), the solutions for $\bar{\Phi}_1$ and $\bar{\Phi}_2$ are then available via Poisson’s integral formula for the half plane

$$\bar{\Phi}_1(\zeta, \eta) = \frac{1}{\pi} \int_{-\infty}^{\infty} \frac{\eta \bar{\Phi}_1(t, 0)}{(\zeta - t)^2 + \eta^2} dt \quad (\text{B 16})$$

$$\bar{\Phi}_2(\zeta, \eta) = -\frac{1}{\pi} \int_{-\infty}^{\infty} \frac{\eta \bar{\Phi}_2(t, 0)}{(\zeta - t)^2 + \eta^2} dt \quad (\text{B 17})$$

The conditions (B 4) and (B 5) indicate that $\bar{\Phi}_1$ and $\bar{\Phi}_2$ are only non-zero on the image of Γ which is the positive real axis ($t \geq 0$) in the ξ -plane. The problem now boils down to determining the function $f(z) := u_1^* = u_2^*$ on Γ such that the stress matching condition (see (2.7) on Γ) holds. Applying this condition is slightly non-trivial because the integrals (B 16) and (B 17) are formally singular for $\xi = \zeta + i\eta$ on Γ . They have well-defined (Cauchy principal) values by continuity with surrounding values of ξ but taking normal derivatives of these integrals and subsequently computing them, nevertheless, requires due care. Consider the normal (η) derivative of $\bar{\Phi}_1$ on Γ ($\eta = 0$), for example. It is

straightforward to show

$$\bar{\Phi}_{1,\eta}(\zeta, \eta) = \frac{1}{\pi} \int_{-\infty}^{\infty} \bar{\Phi}_1(t, 0) \frac{\partial}{\partial t} \left[\frac{\zeta - t}{(\zeta - t)^2 + \eta^2} \right] dt. \quad (\text{B } 18)$$

and, after integration by parts, then

$$\bar{\Phi}_{1,\eta}(\zeta, 0) = \frac{1}{\pi} \int_{-\infty}^{\infty} \frac{\bar{\Phi}_{1,\zeta}(t, 0)}{t - \zeta} dt = \frac{1}{\pi} \int_{-\infty}^{\infty} \frac{\bar{\Phi}_{1,\zeta}(t, 0) - \bar{\Phi}_{1,\zeta}(\zeta, 0)}{t - \zeta} dt \quad (\text{B } 19)$$

since the Cauchy principal value of $\int_{-\infty}^{\infty} 1/(t - \zeta) dt$ is zero. The last integral on the right hand side of (B 19) is now regular. The symmetry of the velocity fields under $y \rightarrow -y$ in the z -plane can then be invoked to make the integration range finite. This reflectional symmetry carries over to the ξ -plane as the symmetry $\bar{\Phi}_i(1/t, 0) = \bar{\Phi}_i(t, 0)$ ($i = 1, 2$) allowing, for example, (B 16) to be simplified to

$$\bar{\Phi}_1(\zeta, \eta) = \frac{\eta}{\pi} \int_0^1 \bar{\Phi}_1(t, 0) \left[\frac{1}{(\zeta - t)^2 + \eta^2} + \frac{1}{(t\zeta - 1)^2 + t^2\eta^2} \right] dt. \quad (\text{B } 20)$$

and (B 19) to

$$\bar{\Phi}_{1,\eta}(\zeta, 0) = \frac{1}{\pi} \int_0^1 \left[\frac{\bar{\Phi}_{1,\zeta}(t, 0) - \bar{\Phi}_{1,\zeta}(\zeta, 0)}{t - \zeta} + \frac{t\bar{\Phi}_{1,\zeta}(t, 0)}{\zeta t - 1} \right] dt + \frac{\bar{\Phi}_{1,\zeta}(\zeta, 0)}{\pi} \log \left(\frac{1 - \zeta}{\zeta} \right). \quad (\text{B } 21)$$

These are the integral representations (along with the equivalent ones for $\bar{\Phi}_2$) used to impose the matching conditions and calculate the flow solution.

In the matching process, the first step in determining f is to construct a global representation, $f(\theta) = \sum_{n=1}^N c_n \Psi_n(\theta)$, using θ to parametrise Γ , c_n as the expansion constants and the basis functions

$$\Psi_n(\theta) := T_{2n}(\theta/\theta_{max}) - T_{2n-2}(\theta/\theta_{max}). \quad (\text{B } 22)$$

These are defined in terms of Chebyshev polynomials $T_n(\theta) := \cos(n \cos^{-1} \theta)$ with each designed to mirror the properties of f : $f(\pm\theta_{max}) = 0$ and $df/d\theta|_{\theta=0} = 0$ by the y -reflectional symmetry. This symmetry also means that the matching condition needs only to be applied (via collocation at the N positive zeros of T_{2N+1}) over the upper half of Γ . It is tempting to carry out this procedure directly in the ξ -plane using the representation (B 21) and the sister integral for $\bar{\Phi}_{2,\eta}$. However, this proves inaccurate because both have an integrable singularity at $t = 0$ ($\theta = \pm\theta_{max}$). This causes loss of accuracy through two separate effects: a) the integrand has a singular derivative at $t = 0$ so numerical quadrature is inefficient and b) the collocation points sparsely populate the neighbourhood of $t = 0$ at extreme choices of α ($\rightarrow 0$ or $\pi/2$) so the matching is not well imposed and convergence fails short of usual spectral (exponential) accuracy. Instead, the integral representations must be transformed to the physical z -plane and matching carried out there.

The velocity profile along Γ is always smooth and typically only $N = 20$ or 30 is needed to see spectral drop off of 4-5 orders of magnitude. The limits $\alpha \rightarrow \pi/2$ and $\alpha \rightarrow 0$, however, have to be treated carefully. For example, when $\alpha \geq 0.2$ ($\approx 10^\circ$) only a 100-panel Simpson quadrature is needed to accurately calculate the integrals along Γ but this must be increased dramatically as $\alpha \rightarrow 0$ due to the extreme behaviour of the $z = z(\xi)$ transformation in this limit (e.g. 10^4 panels proved sufficient for $\alpha = O(0.001)$). Once the solution is obtained, the fluxes Q_1 and Q_2 are calculated using Simpson's rule with typically 20 – 40 panels. This is the most costly part of the process as essentially a

triple integral is being evaluated. Simple bisection in α is used to find a ‘balanced’ flux state where $Q_1 + Q_2 = 0$ for given β , λ and γ .

As a final comment, it’s worth remarking that the transformation $q = q(z)$ (see the third subplot in figure 13) achieves a separation of variables in the problem (the boundaries are contours of constant $r = Re(q)$) and is essentially a transformation to bipolar coordinates. This was the approach taken by Bentwich (1964) and Brauner, Robinsky & Maron (1996) in the unidirectional case. A solution was then developed by separation of variables after a Fourier transform (in s) is taken of the inhomogeneity in the matching condition. This, however, boils down to essentially the same problem of evaluating a triple integral albeit in this case the innermost one for u is an inverse Fourier transform and hence over a semi-infinite interval.

Appendix C. Eccentric solutions

The ‘eccentric’ solution has one fluid completely encapsulated by the other. Bentwich (1964) originally treated this situation for the unidirectional problem by transforming to bipolar coordinates. Here we take a simple conformal transformation approach so as to build an independent code to that used for the side-by-side solutions. Examining the limiting situation of when the encapsulated fluid approaches the pipe wall then allows both codes to cross-validate each other (e.g. see figure 4).

For sake of argument, we describe the solution strategy for A_2 in A_1 . The radius R and centre $(\sigma, 0)$ (with $\sigma < 0$) define the geometry uniquely up to an arbitrary rotation around the duct axis and any reflection about a diameter neither of which, of course, affect the flux. The interface curve Γ is then

$$\Gamma := \{ z \mid z = x + iy = \sigma + Re^{i\theta}; -\pi < \theta \leq \pi \} \quad (\text{C } 1)$$

which smoothly connects to the formula for Γ in the side-by-side solution (formally, R is $+/-$ ve if Γ is convex/concave as viewed from $x = -\infty$: see the definition (B 7)). The problem (2.5)–(2.7) is solved by conformally mapping the geometry of eccentric circles into one of concentric circles using a bilinear transformation $\xi = \xi(z)$. This is constructed by selecting a common pair of real inverse points $(\kappa, 0)$ and $(\nu, 0)$ for Γ and the duct wall $|z| = 1$ (so $|\kappa\nu| = 1$ and $|\kappa - \sigma| |\nu - \sigma| = R^2$) which ensures that the transformation

$$\xi := \frac{z - \kappa}{z - \nu} \quad (\text{C } 2)$$

maps the two circles $|z| = 1$ and Γ into concentric circles of radii (respectively)

$$\varpi_1 := \frac{1 - \kappa}{1 - \nu} \quad \& \quad \varpi_2 := \frac{R + \sigma - \kappa}{R + \sigma - \nu} \quad (\text{C } 3)$$

where

$$\left. \begin{array}{l} \kappa \\ \nu \end{array} \right\} := \frac{\pm(1 + \sigma^2 - R^2) - \sqrt{(1 + \sigma^2 - R^2)^2 - 4\sigma^2}}{2\sigma} \quad (\text{C } 4)$$

(so $\nu < -1$). In the $\xi = \varpi e^{i\phi}$ plane, the solution is found standardly using the expansions

$$u_1 = \sum_{n=1}^N A_n \left(\varpi^n - \frac{\varpi_1^{2n}}{\varpi^n} \right) \cos n\phi + A_0 \log(\varpi/\varpi_1) + \frac{\lambda + 1}{4} (|z|^2 - 1),$$

$$u_2 = \sum_{n=0}^N B_n \varpi^n \cos n\phi + \frac{\lambda - 1}{4\beta} |z|^2$$

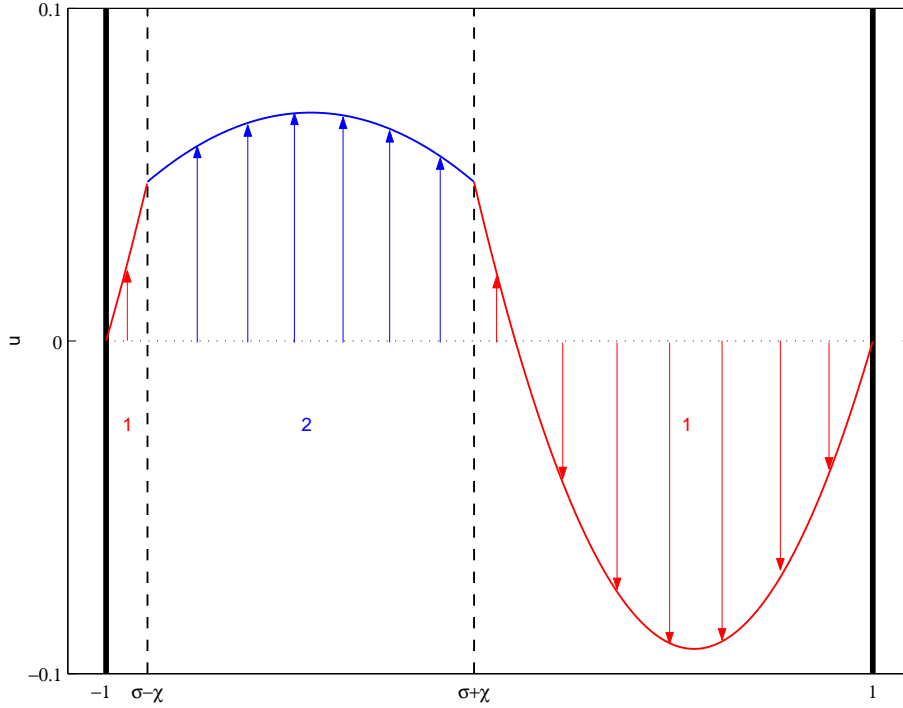


FIGURE 14. The 1D geometry illustrated with the maximal flux solution at $\beta = 5$ ($\lambda = -0.148$, $\sigma = -0.466$, $\chi = 0.426$, $Q_e = 0.0526$). Fluid 1 (flow in red, predominantly down the page) occupies the domain $x \in [-1, \sigma - \chi] \cup [\sigma + \chi, 1]$ and fluid 2 (flow in blue, upwards) occupies $x \in [\sigma - \chi, \sigma + \chi]$.

which incorporate the boundary condition at $|z| = 1$ ($\varpi = \varpi_1$) and the y -symmetry ($\phi \rightarrow -\phi$) of the problem. The Fourier series in ϕ of $|z| = |\nu\xi - \kappa|/|\xi - 1|$ and $\partial|z|/\partial\varpi$ on Γ need to be evaluated to apply the remaining matching conditions. This is done routinely using Simpson's rule with 200 panels when $N = 100$. In the limiting situations of $\sigma - R \rightarrow -1$ (Γ approaching the duct wall) and $\sigma \rightarrow 0$ (approaching concentricity), these numbers are doubled to 400 and $N = 200$ to maintain at worst 10^{-10} least square error in either matching condition. Calculation of the fluxes in A_1 and A_2 is again by 2D Simpson's rule using 100-200 panels per direction and simple bisection is used in R used to identify where $Q_1 + Q_2 = 0$ for given β , λ and $1 + \sigma - R$ ($1 + \sigma - R$ is fixed rather than σ to avoid the complication of multiple solutions).

Appendix D. 1D Analogue

This appendix briefly describes a simple 1D analogue to the 2D problem treated in the main body of the paper. In this, the flow domain is just $x \in [-1, 1]$ and in the most general (eccentric) flow configuration, fluid 2 is in $[\sigma - \chi, \sigma + \chi]$ and fluid 1 is in the complement where χ corresponds to the 'radius' of the encapsulated fluid and σ to the offset (so $\sigma = 0$ recovers a 'concentric' configuration and $\sigma - \chi = -1$ is a side-by-side solution) - see figure 14. As in the main body of the paper, we concentrate on the more viscous fluid - fluid 2 since $\beta \geq 1$ - being encapsulated.

Solving the system defined by equations (2.5)-(2.9) is now a simple exercise in matching

velocity fields which vary quadratically with x ,

$$\begin{aligned} u_1 &= \begin{cases} \frac{1}{2}(\lambda + 1)(x - 1)^2 + A(x - 1) & x \in [\sigma + \chi, 1] \\ \frac{1}{2}(\lambda + 1)(x + 1)^2 + B(x + 1) & x \in [-1, \sigma - \chi] \end{cases} \\ u_2 &= \frac{1}{2\beta}(\lambda - 1)x^2 + Cx + D \quad x \in [\sigma - \chi, \sigma + \chi] \end{aligned} \quad (\text{D } 1)$$

and tangential stresses at the interfaces $x = \sigma \pm \chi$ (4 conditions which specify the constants A, B, C and D). As in the 2D case, the flux balance condition - here given by

$$\begin{aligned} & [(\beta - 1)^2\lambda + \beta(3 - 2\beta) - 1]\chi^4 + \beta[(1 - \beta)\lambda + 2\beta - 1]\chi^3 + 3\beta(\beta - 1)(\sigma^2 + 1)\chi^2 \\ & + \beta[\lambda(1 - \beta) + 1 - 4\beta + 3\sigma^2(\lambda + 1 - \beta\lambda)]\chi + \beta^2(1 + \lambda) = 0, \end{aligned} \quad (\text{D } 2)$$

- determines $\chi(\beta, \lambda)$ uniquely for the concentric solution where $\sigma = 0$ and introduces a constraint between σ and χ in the eccentric flow case. However, in contrast to the 2D situation, the side-by-side solution is also uniquely defined in 1D by balancing the flux (and insisting fluid 2 is bordered by $x = -1$). Put another way, the side-by-side solution is described by one geometry parameter in 1D rather than 2 in the 2D case. The flux for one fluid is then

$$\begin{aligned} Q(\beta, \lambda, \sigma, \chi) &= \frac{1}{3\beta[(\beta - 1)\chi - \beta]} \left[(\beta - 1)(\lambda - 5)\chi^4 + (\beta(17 - \lambda) - 12)\chi^3 \right. \\ &\quad \left. + \left(3\sigma^2(\lambda(1 - \beta) + \beta + 3) + 3\lambda(1 - \beta) - 21\beta + 9 \right) \chi^2 \right. \\ &\quad \left. - \left(3\sigma^2(2 + 2\lambda + \beta - \beta\lambda) + 2\lambda - 5\beta\lambda - 11\beta + 2 \right) \chi - 2\beta(1 + \lambda) \right] \end{aligned} \quad (\text{D } 3)$$

Figure 15 (the 1D analogue of figure 6) shows how $\max_\lambda Q$ varies as a function of the distance $d := \sigma - \chi + 1$ of fluid 2 from the boundary at $x = -1$ for a few different β . Because the side-by-side solution corresponds to just one point in this plot, it is now only the global flux maximiser at $\beta = 1$. As soon as $\beta > 1$, an eccentric solution becomes the global flux maximiser in a smooth transition where the optimal value of $d := \sigma - \chi + 1$ increases continuously from 0. Figure 16 summarises the 1D findings (compare with figure 9). Here, $\max_\lambda Q_s$ and $\max_\lambda Q_c$ appear $O(1/\beta)$ whereas $\max_{\lambda, d} Q_e$ and $\max_\lambda Q_c$ remain $O(1)$ as $\beta \rightarrow \infty$. The key feature of the 2D calculations is therefore recovered in this simplified 1D situation: the global maximiser of flux is never the symmetric ('concentric core-annular') solution, being instead either the side-by-side solution at low β (here precisely $\beta = 1$) or an eccentric core-annular solution at large β (here $\beta > 1$).

REFERENCES

- ARAKERI, J.H., AVILA, F.E., DADA, J.M. & TOVAR, R.O. 2000 Convection in a long vertical tube due to unstable stratification- A new type of turbulent flow? *Current Science* **79**, 859-866.
- BATCHELOR, G.K. & NITSCHKE, J.M. 1993 Instability of stratified fluid in a vertical cylinder. *J. Fluid Mech.* **252**, 419-448.
- BECKETT, F., MADER, H.M., PHILLIPS, J.C., RUST, A. & WITHAM, F. 2011 An experimental study of low Reynolds number exchange flow of two Newtonian fluids in a vertical pipe. *J. Fluid Mech.* submitted.
- BENTWICH, M. 1964 Two-phase viscous axial flow in a pipe *Trans ASME D* **86**, 669-672.
- BENTWICH, M. 1976 Two-phase axial laminar flow in a pipe with naturally curved surface *Chem. Eng. Sci.* **31**, 71-76.

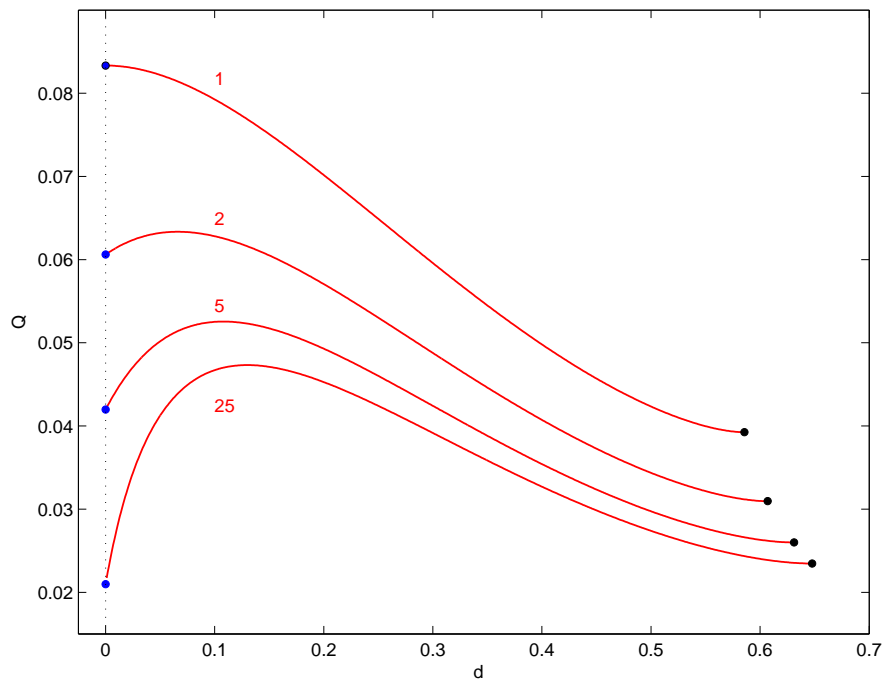


FIGURE 15. $\max_{\lambda} Q$ as a function of $d := \sigma - \chi + 1$ for $\beta = 1, 2, 5$ and 25 in the 1D model. The single dot at the ends of each curve corresponds to the side-by-side case Q_s (left: $d = 0$) and to the concentric case Q_c (right). The global flux maximum is a side-by-side solution for $\beta = 1$ and an eccentric solution for $\beta > 1$.

- BENTWICH, M., KELLY, D.A.I. & EPSTEIN, N. 1970 Two-phase eccentric interface laminar pipeline flow *J. Basic Eng.* **92**, 32-36.
- BIBERG, D. & HALVORSEN, G. 2000 Wall and interfacial shear stress in pressure driven two phase laminar stratified pipe flow in circular conduits *Int. J. Multiphase Flow* **26**, 1645-1673.
- BRAUNER, N., ROVINSKY, J. & MARON, D.M. 1996 Analytical solution for laminar-laminar two-phase stratified flow in circular conduits *Chem. Eng. Comm.* **141-142**, 103-143.
- CHARLES, M.E. & REDBERGER, P.J. 1961 The reduction of pressure gradients in oil pipelines by the addition of water. Numerical analysis of stratified flows *Can. J. Chem. Engng* **40**, 70-75.
- EVERAGE, A.E. 1973 Theory of bicomponent flow of polymer melts.I Equilibrium Newtonian tube flow *Trans. Soc. Rheol.* **17**, 629-646.
- FRIGAARD, I.A. & SCHERZER, O. 1998 Uniaxial exchange flows of Bingham fluids in a cylindrical duct *IMA J. App. Math.* **61**, 237-266.
- GEMMELL, A.R. & EPSTEIN, N. 1962 Numerical Analysis of stratified laminar flow of two immiscible Newtonian liquids in a circular pipe *Can. J. Chem. Eng.* **40**, 215-224.
- GOODMAN, J., KOHN, R.V. & REYNA, L. 1986 Numerical study of a relaxed variational problem from optimal design *Comput. Meth. Appl. Mech. Eng.* **57**, 107-127
- GORELIK, D. & BRAUNER, N. 1999 The interface configuration in two-phase stratified pipe flows. *Int. J. Multiphase Flow* **25**, 977-1007.
- HALL, A.R.W. 1992 Multiphase flow of oil, water and gas in horizontal pipes. *PhD thesis*, University of London.
- HALL, A.R.W. & HEWITT, G.F. 1993 Application of two-fluid analysis to laminar stratified oil-water flows *Int. J. Multiphase Flow* **19**, 711-717.

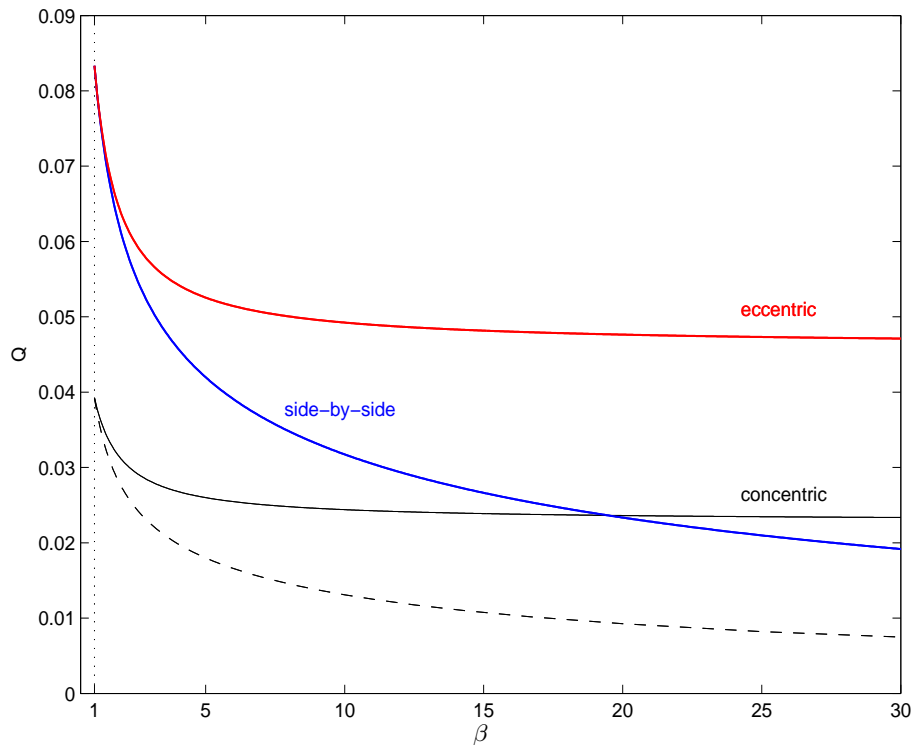


FIGURE 16. $\max_{\lambda} Q_s$ (blue second highest curve at $\beta = 10$), $\max_{\lambda,d} Q_e$ (upper red curve) and $\max_{\lambda} Q_c$ (lowest solid black curve) compared as a function of β in the 1D model. The lowest dashed (black) curve corresponds to $\max_{\lambda} \hat{Q}_c$.

- HASSON, D., MANN, U. & NIR, A. 1970 Annular flow of two immiscible liquids. I. Mechanisms. *Can. J. Chem. Engng.* **48**, 514.
- HODGSON, G.W. & CHARLES, M.E. 1963 The pipeline flow of capsules. Part 1: The concept of capsule pipelining *Can. J. Chem. Engng.* **41**, 43-45.
- HUPPERT, H.E. & HALLWORTH, M.A. 2007 Bi-directional flows in constrained systems *J. Fluid Mech.* **578**, 95-112.
- JOSEPH, D.D., RENARDY, M. & RENARDY, Y. 1984 Instability of the flow of two immiscible liquids with different viscosities in a pipe. *J. Fluid Mech.* **141**, 309-317.
- JOSEPH, D.D., NGUYEN, K. & BEAVERS, G.S. 1984 Non-uniqueness and stability of the configuration of flow of immiscible fluids with different viscosities. *J. Fluid Mech.* **141**, 319-345.
- JOSEPH, D.D., BAI, R., CHEN, K.P. & RENARDY, Y.Y. 1997 Core-annular flows *Ann. Rev. Fluid Mech.* **29**, 65-90.
- KAZAHAYA, K. SHINOHARA, H. AND SAITO, G. 1994 Excessive degassing of Izu-Oshima volcano: magma convection in a conduit *Bull. Volcanol.* **56**, 207-216.
- KRUYER, J., REDBERGER, P.J. & ELLIS, H.S. 1967 The pipeline flow of capsules. Part 9. *J. Fluid Mech.* **30**, 513-531.
- LEE, B.L. & WHITE, J.L. 1974 An experimental study of rheological properties of polymer melts in laminar shear flow and of interface deformation and its mechanisms in two-phase stratified flow. *Trans. Soc. Rheol.* **18**, 467.
- MACLEAN, D.L. 1973 A theoretical analysis of bicomponent flow and the problem of interface shape *Trans. Soc. Rheol.* **17**, 385.

- MARKUSKEVICH, A. I. 1965 Theory of Functions of a Complex Variable, vol 1 *Prentice-Hall, Inc.* Englewood Cliffs, New Jersey (p205-207)
- MINAGAWA, N. & WHITE, J.L. 1975 Coextrusion of unfilled and TiO₂-filled polyethylene: influence of viscosity and die cross-section on interface shape. *Polymer Engng Sci.* **15**, 825.
- MOYERS-GONZALEZ, M.A. & FRIGAARD, I.A. 2004 Numerical solution of duct flows of multiple visco-plastic fluids *J. Non-Newtonian Fluid Mech.* **122**, 227-241.
- NG, T.S., LAWRENCE, C.J. & HEWITT, G.F. 2002 Laminar stratified pipe flow *Int. J. Multiphase Flow.* **28**, 963-996.
- PACKHAM, B.A. & SHAIL, R. 1971 Stratified laminar flow of two immiscible fluids *Proc. Camb. Phil. Soc.* **69**, 443-448.
- RANGER, K.B. & DAVIS, A.M.J. 1979 Steady pressure driven two-phase stratified laminar flow through a pipe *Can. J. Chem. Eng.* **57**, 688-691.
- ROVINSKY, J., BRAUNER, N. & MARON, D.M. 1997 Analytical solution for laminar two-phase flow in a fully eccentric core-annular configuration *Int. J. Multiphase Flow* **23**, 523-543.
- SEMENOV, N.L. & TOCHIGIN, A.A. 1962 An analytical study of the separate laminar flow of a two-phase mixture in inclined pipes *J. Eng. Phys.* **4**, 29.
- SEON, T., ZNAIEN, J., SALIN, D., HULIN, J.P., HINCH, E.J. & PERRIN, B. 2007 Transient buoyancy-driven front dynamics in nearly horizontal tubes *Phys. Fluids* **19**, 123603
- SOUTHERN, J.H. & BALLMAN, R.L. 1973 Stratified bicomponent flow of polymer melts in a tube *Appl. Polymer Symp.* **20**, 175-189.
- STEVENSON, D.S. & BLAKE, S. 1998 Modelling the dynamics and thermodynamics of volcanic degassing *Bull. Volcanol.* **60**, 307-317.
- TAGHAVI, S.M., SEON, T., MARTINEZ, D.M. & FRIGAARD, I.A. 2009 Buoyancy-dominated displacement flows in near-horizontal channels: the viscous limit *J. Fluid Mech.* **639**, 1-35.
- VLASOV, V.I. 1986 Solution of a Dirichlet problem in a crescent-shaped domain *J. Eng. Phys. & Thermophys.* **50**, 741-747.
- WHITE, F. M. Viscous Fluid Flow *McGraw-Hill* (p124) 1991
- WILLIAMS, M.C. 1975 Migration of two liquid phases in capillary extrusion: an energy interpretation *AIChE. J.* **21**, 1204.
- YU, H.S. & SPARROW, E.M. 1967 Straified laminar flow in ducts of arbitrary shape *AIChE. J.* **13**, 10.
- ZNAIEN, J., HALLEZ, Y., MOISY, F., MAGNAUDET, J., HULLIN, J.P., SALIN, D. & HINCH, E.J. 2009 Experimental and numerical investigations of flow structure and momentum transport in a turbulent buoyancy-driven flow inside a tilted tube. *Phys. Fluids* **21**, 115102.